[redacted]

NATIONAL AERONAUTICS AND SPACE ADMINISTRATION

TECHNICAL MEMORANDUM X-279

EFFECT OF SEVERAL TAIL CONFIGURATIONS ON THE STABILITY CHARACTERISTICS OF A MIDWING SUPERSONIC-BOMBER MODEL AT MACH NUMBERS OF 1.60, 1.90, 2.20, AND 2.50*

By R. Franklin Wells and H. Norman Silvers

SUMMARY

A midwing supersonic-bomber model was investigated in the Langley Unitary Plan wind tunnel to determine the effect of several tail configurations on longitudinal and lateral stability characteristics at Mach numbers of 1.60, 1.90, 2.20, and 2.50.

The fuselage had a fineness ratio of 12.810. The wing had an aspect ratio of 3.20, a taper ratio of 0.40, dihedral of -8°, and 21.8° sweep of the quarter chord. The tails consist of two basic types, a T-tail configuration and a low-tail configuration. Various modifications of the T-tail configuration were obtained by the addition of the following components to the basic T-tail: single ventral fin. dual ventral fins, extended nacelles, and wedges on the vertical tail. Two values of dihedral were used on the low horizontal tail, -10° and -30°. In addition, wedges on the vertical tail and rudder deflections were tested with the low-tail configuration.

The T-tail configuration exhibited a destabilizing tendency of the pitching-moment-coefficient curve at the higher angles of attack. The low-tail configuration showed no abrupt change in longitudinal stability and the stability tended to be unaffected by Mach number. The T-tail configuration has more effective directional stability at the high angles of attack than the low-tail configuration. Dual ventral fins were more effective than a single ventral fin in increasing directional stability of the T-tail at high angles of attack and high Mach number.

*Title, Unclassified.

INTRODUCTION

An investigation was made of the aerodynamic characteristics of a model of a supersonic tactical bomber. Basically the mission of such airplanes calls for a subsonic cruise with a supersonic dash capability at Mach numbers approaching 3. The purpose of the investigation was to determine a tail configuration which would have acceptable longitudinal and lateral stability characteristics and directional control over the supersonic part of the mission.

Several different tail arrangements believed to have good aerodynamic characteristics and to be feasible from the construction standpoint were selected. Time did not permit progressive modifications to be made in order to arrive at a completely satisfactory solution of the problems.

A T-tail in conjunction with a single and dual ventral fin and low tail with a horizontal-tail dihedral of -10° and -30° were tested. The rudder effectiveness was determined for several controls on the T-tail configuration.

The present paper presents results obtained at Mach numbers of 1.60, 1.90, 2.20, and 2.50 in the Langley Unitary Plan wind tunnel.

The results of this investigation are presented as a brief evaluation of the longitudinal and lateral stability characteristics of the model with several arrangements of the stabilizing surfaces.

Because of the lack of sufficient corrective drag measurements, drag coefficients are not presented.

COEFFICIENTS AND SYMBOLS

All longitudinal results are presented about the stability system of axes and all lateral results are presented about the body system of axes. These systems are illustrated in figure 1.

The reference point for all moments is located in the chord plane of the wing at 25 percent of the wing mean geometric chord.

b wing span, in.

C_L lift coefficient, $\frac{\text{Lift}}{qS}$

[redacted]

C_{L_α}	lift-curve slope, $\frac{\partial C_L}{\partial \alpha}$, $\left(C_L \approx 0\right)$
C_Y	side-force coefficient, $\frac{\text{Side force}}{qS}$
C_{Y_β}	slope of side-force curve, $\frac{\partial C_Y}{\partial \beta}$, $(\beta \approx 0)$
C_l	rolling-moment coefficient, $\frac{\text{Rolling moment}}{qSb}$
C_{l_β}	effective-dihedral parameter, $\frac{\partial C_l}{\partial \beta}$, $(\beta \approx 0)$
C_m	pitching-moment coefficient, $\frac{\text{Pitching moment}}{qS\bar{c}}$
$C_{m_{C_L}}$	slope of pitching-moment curve, $\frac{\partial C_m}{\partial C_L}$, $\left(C_L \approx 0\right)$
$C_{m,o}$	pitching moment at zero lift
C_n	yawing-moment coefficient, $\frac{\text{Yawing moment}}{qSb}$
C_{n_β}	directional-stability parameter, $\frac{\partial C_n}{\partial \beta}$, $(\beta \approx 0)$
$C_{n_{\delta_r}}$	rudder effectiveness parameter, $\frac{\partial C_n}{\partial \delta_r}$, $\left(\delta_r \approx 0\right)$
$c/4$	quarter chord
$\bar{c}$	wing mean geometric chord, in.
M	free-stream Mach number
q	free-stream dynamic pressure, lb/sq ft

[redacted]

S	wing area including body intercept, sq ft
X,Y,Z	body axes, (see fig. 1(b))
X_s, Y_s, Z_s	stability axes (see fig. 1(a))
α	angle of attack, referred to the chord plane of the wing uncorrected for tunnel flow angularity, deg
$\alpha_{o,corr}$	angle of attack at zero lift corrected for tunnel flow angularity, deg
β	angle of sideslip, referred to fuselage center line, deg
Γ_t	dihedral angle of the horizontal tail, deg
δ_r	rudder deflection measured perpendicular to the hinge line, deg
ϕ	angle of roll, 0^o with model wing vertical, deg

APPARATUS AND MODELS

The tests were conducted in the low Mach number test section of the Langley Unitary Plan wind tunnel. This tunnel is a variable pressure, continuous-flow type. The test section is 4 feet square and approximately 7 feet in length. The nozzle leading to the test section is of the asymmetric sliding-block type and the Mach number may be varied continuously through a range from approximately 1.6 to 2.8 without tunnel shutdown.

Details of the model and model components are shown in figures 2 to 4. The geometric characteristics of the model are given in table I. Photographs of the model are presented as figure 5.

The model consists of a low-aspect-ratio wing mounted in a mid-height location on the fuselage-nacelle combination. The nacelles, located on the sides of the fuselage, had inlets which were of the two-dimensional, external-compression type utilizing a boundary-layer bleed adjacent to the fuselage sides. Air was ducted from the inlets through the nacelles to two circular exits on either side of the fuselage. The exits were located forward of the fuselage base. Nacelle extensions were provided for the model and attached to the original exits extending them rearward along the fuselage as shown in figures 2(b) and 5(d).

The wing, shown in figure 2(a), has 21.8° sweep of the quarter-chord line, aspect ratio of 3.20, taper ratio of 0.40, and a 3.5-percent-thick biconvex airfoil section. The wing had a dihedral angle of -8°.

Two basic tail arrangements were provided for the model. One arrangement, called herein the T-tail, consisted of a vertical tail of aspect ratio 0.976 with a quarter-chord line swept back 60.0° and the horizontal tail located in a high position on the vertical tail. Details of the T-tail configuration are shown in figure 3. The second tail arrangement, called herein the low tail, consisted of a vertical tail of aspect ratio 0.913 with a quarter-chord line swept back 54.6° and the horizontal tail mounted on the lower portion of the nacelle extensions. This horizontal tail was tested with dihedral angles of -10.0° and -30.0°. Details of the low-tail configuration are shown in figure 4. All tail-surface airfoil sections were formed by wedge-type leading- and trailing-edge sections joined with a thin parallel-sided midsection.

The T-tail configuration was tested with a flap-type rudder deflected to an angle of 19° with respect to the vertical-tail chord plane. A wedge block was also provided for one side of the vertical tail of the T-tail to introduce an effect of rudder deflection. The wedge, shown in figure 3, when attached to the vertical tail formed an angle of 12.0° with the chord plane of the vertical tail. A wedge block was also provided for the vertical tail of the low-tail configuration. This wedge, shown in figure 4, when attached to the vertical tail formed an angle of 30.0° with the chord plane of the vertical tail.

Two arrangements of ventral fins were investigated with the T-tail configuration. One arrangement consisted of dual ventral fins located on the bottom of the fuselage and rotated 30.0° from the plane of symmetry (figs. 2(a) and 3). The other arrangement consisted of a single ventral fin below the fuselage with the chord plane in the plane of symmetry (figs. 2(a) and 3).

Forces and moments for the model were measured by a six-component internal strain-gage balance attached by means of a sting to the tunnel support system. Included in the tunnel support system was a remotely operated adjustable-angle coupling that permitted tests to be made at variable angles of attack concurrently with variations in the angle of sideslip.

TESTS

Tests were made through an angle-of-attack range that extended from about -4° to about 18° at 0° and -4° angles of sideslip. To obtain the lateral stability parameters, increments were taken between lateral

results obtained at $\beta = 0^\circ$ and $\beta = -4^\circ$. This incremental method of obtaining the lateral stability parameters through the angle-of-attack range is valid if the lateral stability characteristics of the model are linear within the range of sideslip angles at which the tests were made ($\beta = 0^\circ$ and -4°). To indicate this linearity of the lateral characteristics with angle of sideslip as well as to determine the lateral characteristics at higher angles of sideslip, some tests were also made (for angles of attack of 0°, 9°, and 18°) through an angle-of-sideslip range that extended from about 4° to -18°. The tests were made generally at Mach numbers of 1.60, 1.90, 2.20, and 2.50. Some configurations were, however, investigated at only selected conditions of the aforementioned attitudes and Mach numbers. A summary of the test conditions for the various model configurations is presented as table II.

The test conditions of stagnation pressure, dynamic pressure, and Reynolds number corresponding to the test Mach numbers are given in the following table:

M	Stagnation pressure, lb/sq in. abs	Dynamic pressure, lb/sq ft	Reynolds number
1.60	5.00	304.01	0.586×10^6
1.90	5.60	305.02	.590
2.20	6.60	301.00	.607
2.50	8.15	301.65	.647

The Reynolds number is based on the mean geometric chord of the wing.

The dewpoint for all tests was maintained below -30° F to prevent adverse condensation effects. The stagnation temperature was maintained at 125° F for all Mach numbers.

CORRECTIONS AND ACCURACY

At the time of the tests, the tunnel had not been completely calibrated, and the amount of flow angularity was not known. Thus, no angularity corrections were applied to the basic data. It has since been determined that upflow angles of 0.4°, 0.8°, 1.5°, and 1.1° exist at Mach numbers of 1.60, 1.90, 2.20, and 2.50, respectively. Only the summary plots of $\alpha_{o,corr}$ have been corrected for flow angularity.

The maximum deviation of local Mach number in the portion of the tunnel occupied by the model was ±0.015 from the average values listed. The angles of attack and sideslip have been corrected for the deflection of the support system under load.

The estimated accuracy of the force and moment coefficients, based on balance calibration and repeatability of the data, is within the following limits:

C_L	±0.0100
C_m	±0.0010
C_l	±0.0005
C_n	±0.0001
C_Y	±0.0025
α, deg	±0.1
β, deg	±0.1
δ_r, deg	±0.1

Based on the accuracy of these coefficients and angles and values of the parameters measured, the estimated accuracy of the lateral parameters computed from increments of coefficients and angles is:

C_{l_β}	±0.0004
C_{n_β}	±0.0004
C_{Y_β}	±0.0015

PRESENTATION OF RESULTS

The results of this investigation are presented in the following figures:

	Figures
Schlieren photographs	6 to 8
Longitudinal aerodynamic characteristics of the model with various tail configurations:	
T-tail	9(a)
T-tail with dual ventral fins	9(b)
T-tail, $\delta_r = 19^\circ$	9(c)
T-tail with extended nacelle, $\delta_r = 19^\circ$	9(d)
T-tail without horizontal tail, $\delta_r = 19^\circ$	9(e)
T-tail with 12° wedge	9(f)

	Figures
Model without tail	9(g)
Low tail, $\Gamma_t = -10^\circ$	9(h)
Low tail, $\Gamma_t = -30^\circ$	9(i)
Vertical tail of low-tail configuration and 30° wedge (without horizontal tail)	9(j)
Summary of longitudinal aerodynamic characteristics:	
T-tail with and without ventral fins	10
T-tail and low tail	11
Summary of lateral aerodynamic characteristics:	
T-tail with and without ventral fins	12
T-tail and low tail	13
Rudder effectiveness	14

DISCUSSION

The longitudinal stability of the basic T-tail configuration at high angles of attack decreased rapidly with increase in lift coefficient and became neutral at a lift coefficient of about 0.9 for all test Mach numbers (fig. 9(a)). This is evidently a result of adverse downwash conditions at this horizontal-tail location since the tail-off-configuration pitching moments are essentially linear to the highest test lift coefficients (fig. 9(g)). The use of dual ventral fins has no appreciable effect on the pitching-moment coefficients. (See fig. 9(b).) Extension of the nacelles (fig. 9(d)) reduced the nonlinearity of the pitching-moment curves at high lift coefficients markedly. The pitching-moment curves for the low tail (figs. 9(h), 9(i), and 9(j)) were essentially linear to the highest lift coefficients tested. The low-tail configuration exhibited greater longitudinal stability than the T-tail at the two Mach numbers shown in figure 11.

The directional stability of all configurations decreased with increase in Mach number or angle of attack as is usual. At low angles of attack, the single and dual ventral fins were equally effective in increasing the directional stability of the model (fig. 12). At high angles of attack, the single ventral fins contributed considerably less to the directional stability than the dual fins. At a Mach number of 2.50, the dual fins increased the angle of attack at which the directional stability becomes zero from 10.5° to 16.3°. The low-tail configuration (fig. 13) with either -10° or -30° of dihedral had greater directional stability than the T-tail arrangement at low angles of attack. The reverse was true at angles of attack above 10°.

Rudder effectiveness (fig. 14) for the T-tail configuration was essentially zero below an angle of attack of 6°. As angle of attack was increased above this value, the effectiveness increased. The effectiveness at low angles of attack was improved by removal of the horizontal tail.

Langley Research Center,
National Aeronautics and Space Administration,
Langley Field, Va., January 14, 1960.

TABLE I

GEOMETRIC CHARACTERISTICS OF SUPERSONIC-BOMBER MODEL

	Wing	T-tail configuration				Low-tail configuration		
		Vertical tail	Horizontal tail	Ventral fins		Vertical tail	Horizontal tail	
				Dual	Single		Dihedral -10°	Dihedral -5°
Area, sq ft	[a]0.547	0.104	[b]0.078	[c]0.029	0.028	0.081	[d]0.059	[d]0.062
Span, ft	[a]1.325	0.319	0.521	[e]0.183	0.144	0.373	[f]0.299	[f]0.280
Mean geometric chord, ft	0.438	0.329	0.163			0.333	0.218	0.218
Aspect ratio	3.20	0.976	3.500	1.199	0.740	0.915	1.000	2.000
Taper ratio	0.40	0.766	0.300	0.927	0.415	0.256	0.500	0.500
Tail length[g], ft		1.008	1.500			1.042	0.829	0.850
Sweep angle of -								
Leading edge, deg	28.1	60.9	31.6	55.7	69.7	59.9	55.7	55.7
Quarter-chord, deg	21.8	60.0	24.8			54.6	27.0	30.1
Trailing edge, deg	0.0	56.8	0.0	30.8	60.4	25.4	-1.9	-2.3
Dihedral, deg	-8.0		0.0	-90.0			-10.0	-30.0
Incidence, deg	2.0		5.0	0.0	0.0		4.0	-4.0
Percent thickness at:								
Root chord	3.5	4.8	2.5	2.9	2.3	1.8	7.1	7.1
Tip chord	3.5	5.9	5.9	4.2	4.6	5.1	9.1	9.1
Airfoil section:								
Root	Modified biconvex	Modified double wedge	Modified double wedge			Modified double wedge		
Tip			Double wedge			Double wedge		

Fuselage:	
Maximum diameter, ft	0.217
Length, ft	2.772
Base area, sq ft	0.0125
Fineness ratio	1.0810
Volume, cu ft	0.0476
Nacelles:	
Length, ft	1.1017
Inlet area, sq ft	0.0467
Exit area, sq ft	0.0855
Base area, sq ft	0.1064
Thrust angle, deg	-6.5
Extended nacelles:	
Length, ft	1.2650
Inlet area, sq ft	0.0467
Exit area, sq ft	0.0855
Base area, sq ft	0.1064

[a]Projected to horizontal, includes portion in fuselage total area.

[b]Total area.

[c]Theoretical root chord, single panel.

[d]Exposed area, projected to horizontal, single panel.

[e]Single panel.

[f]Length projected to horizontal, single panel.

[g]Measured from c/4 of mean geometric chord of horizontal tail to c/4 of mean geometric chord of wing.

TABLE II

MODEL TEST CONDITIONS

Configuration	Test Mach numbers for -				
	$\alpha \approx -4^\circ$ to 18°		$\beta \approx -18^\circ$ to 4°		
	$\beta \approx 0^\circ$ (pitch run)	$\beta \approx -4^\circ$ (parameter run)	$\alpha \approx 0^\circ$	$\alpha \approx 9^\circ$	$\alpha \approx 18^\circ$
T-tail	1.6, 1.9, 2.2, 2.5	1.6, 1.9, 2.2, 2.5	1.9, 2.2, 2.5	1.6, 1.9, 2.2, 2.5	1.6, 1.9, 2.2, 2.5
T-tail with dual ventral fins	1.6, 1.9, 2.2, 2.5	1.6, 1.9, 2.2, 2.5	1.9, 2.2, 2.5	1.6, 1.9, 2.2, 2.5	1.6, 1.9, 2.2, 2.5
T-tail with single ventral fin	----------	1.6, 1.9, 2.2, 2.5	1.6, 2.5	1.6, 2.5	1.6, 2.5
T-tail, $\delta_r = 19^\circ$	1.6, 1.9, 2.2, 2.5	----------	----------	----------	----------
T-tail with extended nacelle, $\delta_r = 19^\circ$	1.6, 1.9, 2.2	----------	----------	----------	----------
T-tail without horizontal tail, $\delta_r = 19^\circ$	1.6, 2.5	----------	----------	----------	----------
T-tail with 12° wedge	1.9, 2.5	----------	----------	----------	----------
Model without tail	1.6, 1.9, 2.2, 2.5	1.6, 1.9, 2.2, 2.5	----------	1.6, 2.5	----------
Low tail, $\Gamma_t = -10^\circ$	1.6, 2.5	1.6, 2.5	2.5	----------	1.6, 2.5
Low tail, $\Gamma_t = -30^\circ$	1.6, 2.5	1.6, 2.5	2.5	1.6	1.6, 2.5
Vertical tail of low-tail configuration and 30° wedges (without horizontal tail)	1.6, 1.9, 2.2, 2.5	----------	----------	----------	----------

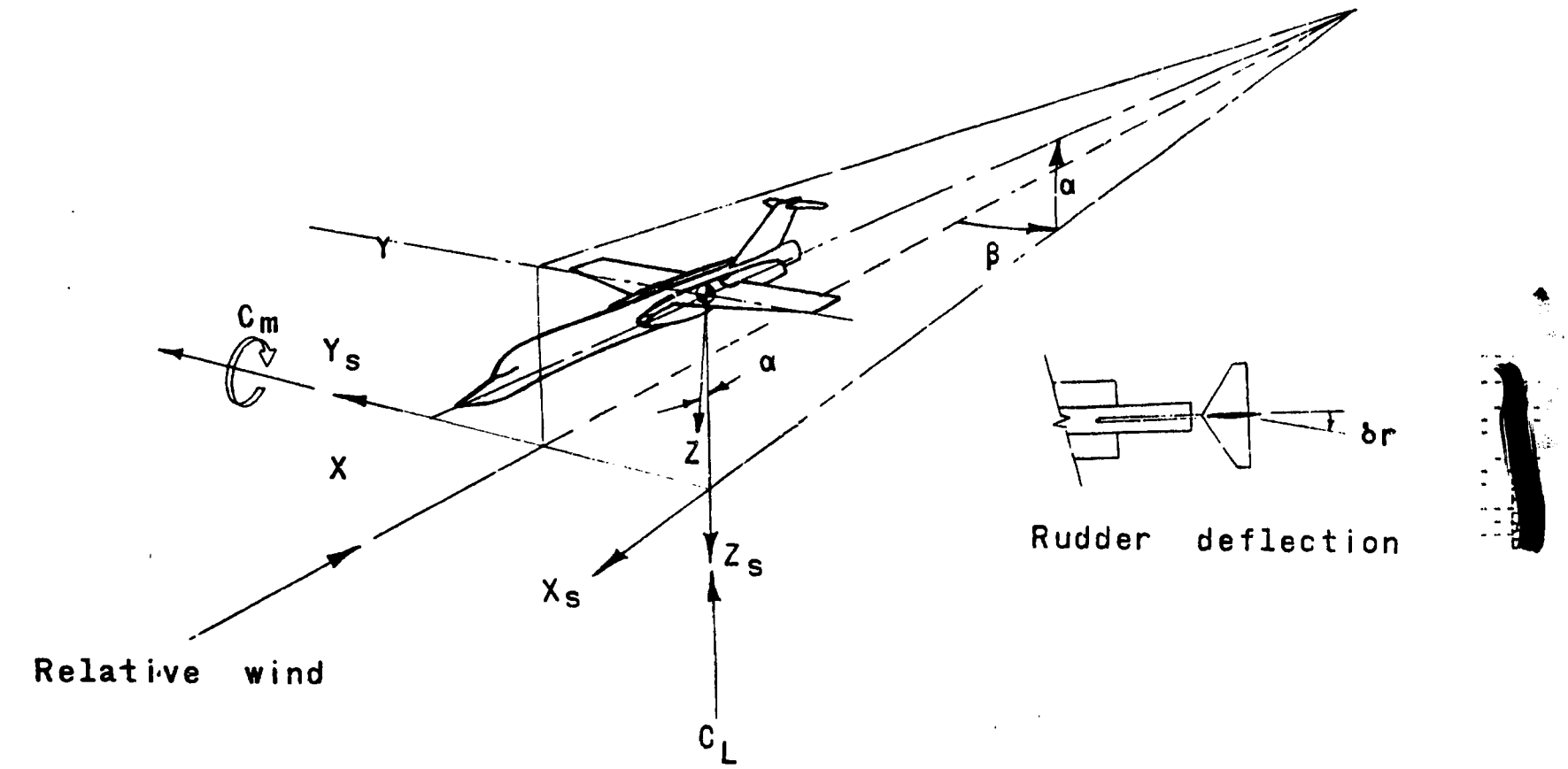

(a) Stability axis.

Figure 1.- Axis systems. Positive values of forces, moments, and angles are indicated by arrows.

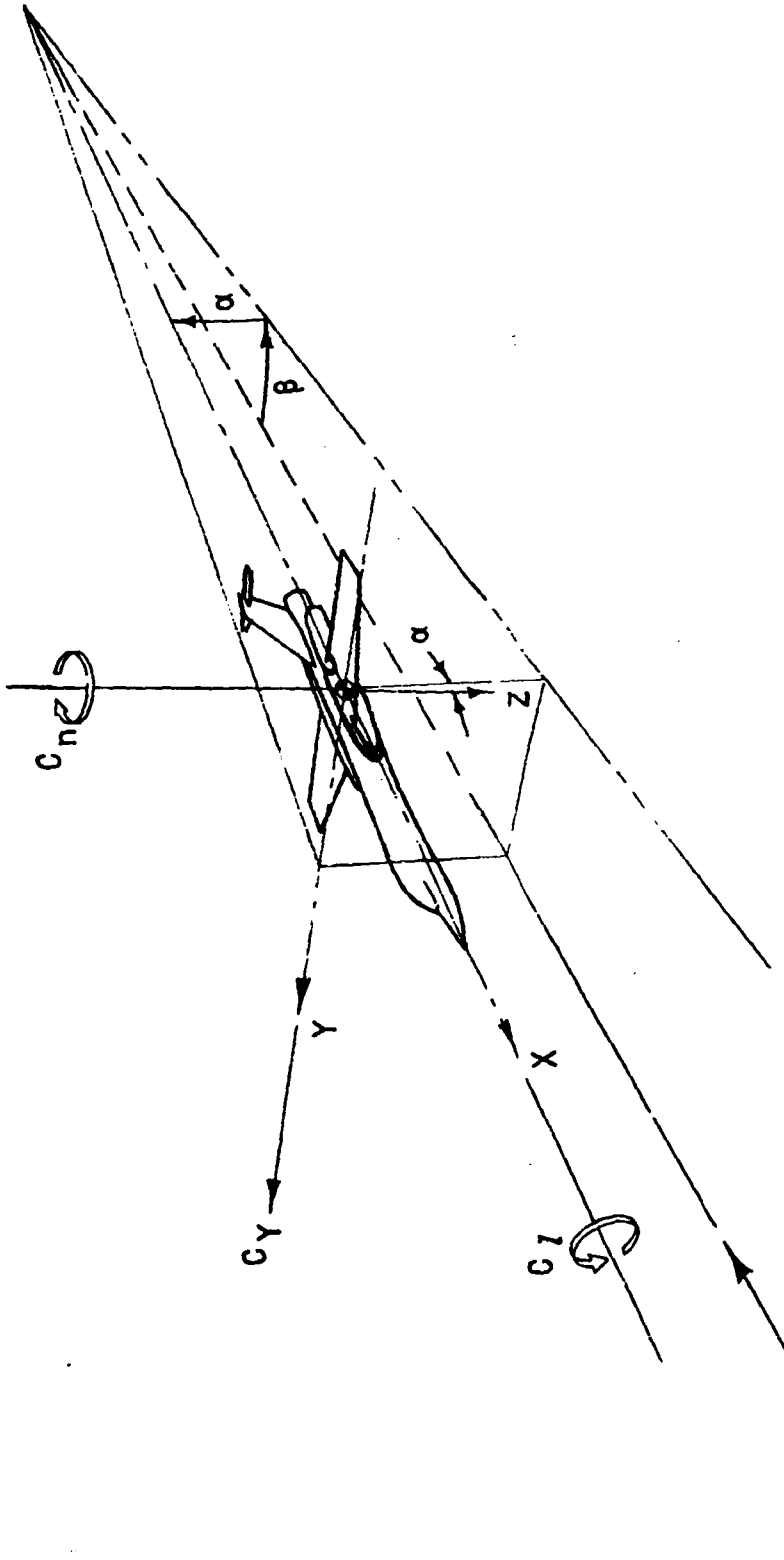

(b) Body axis.

Figure 1.- Concluded.

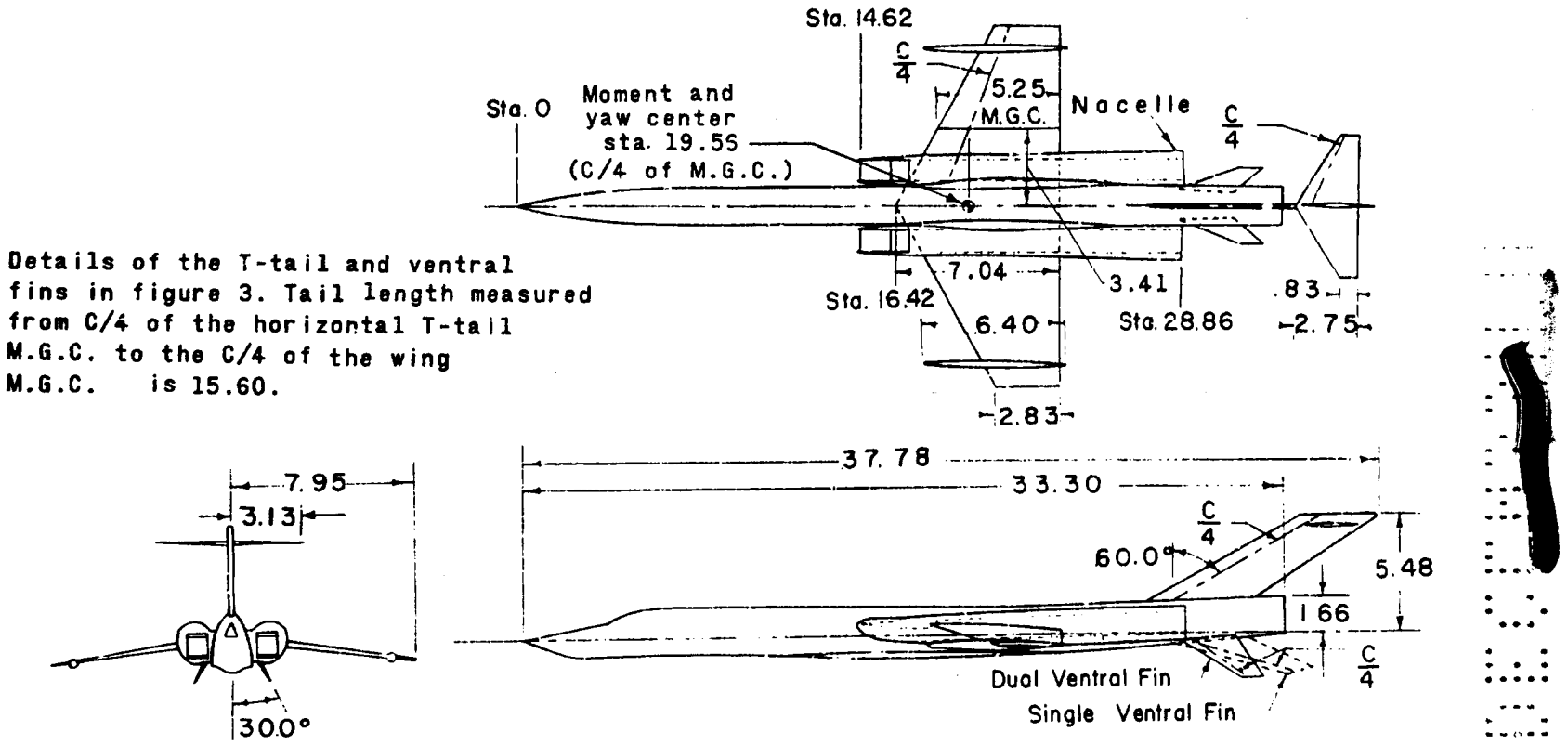

Details of the T-tail and ventral fins in figure 3. Tail length measured from C/4 of the horizontal T-tail M.G.C. to the C/4 of the wing M.G.C. is 15.60.

(a) T-tail configuration.

Figure 2.- Details of general arrangement of the supersonic-bomber model. All dimensions are in inches.

Full details of wing-fuselage-duct combination in figure 2(a). Details of the low-tail in figure 4. Tail length measured from C/4 of the horizontal low-tail M.G.C. to the C/4 of the wing M.G.C. is 9.78 for -10° dihedral tail and 9.84 for -30° dihedral tail.

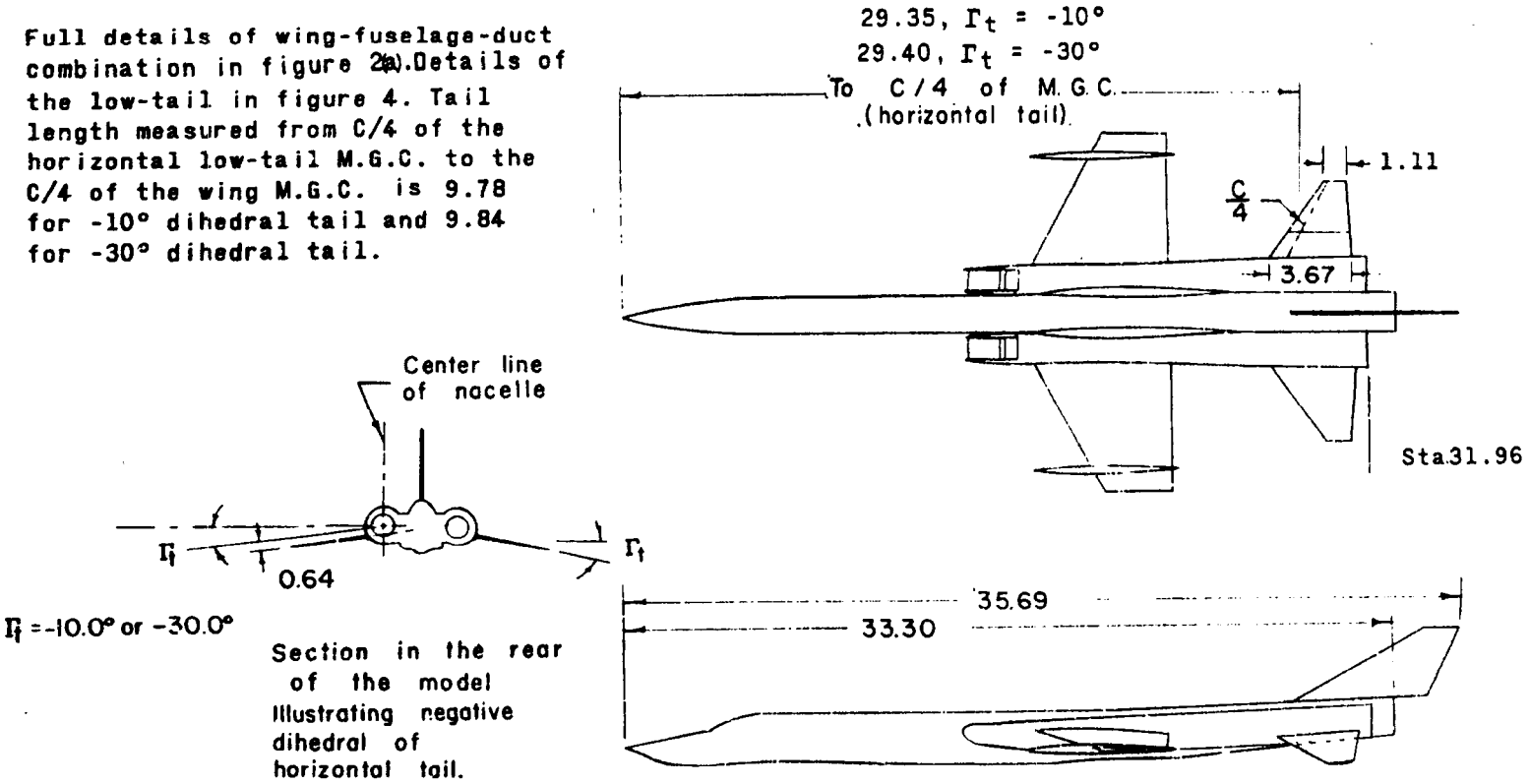

(b) Low-tail configuration.

Figure 2.- Concluded.

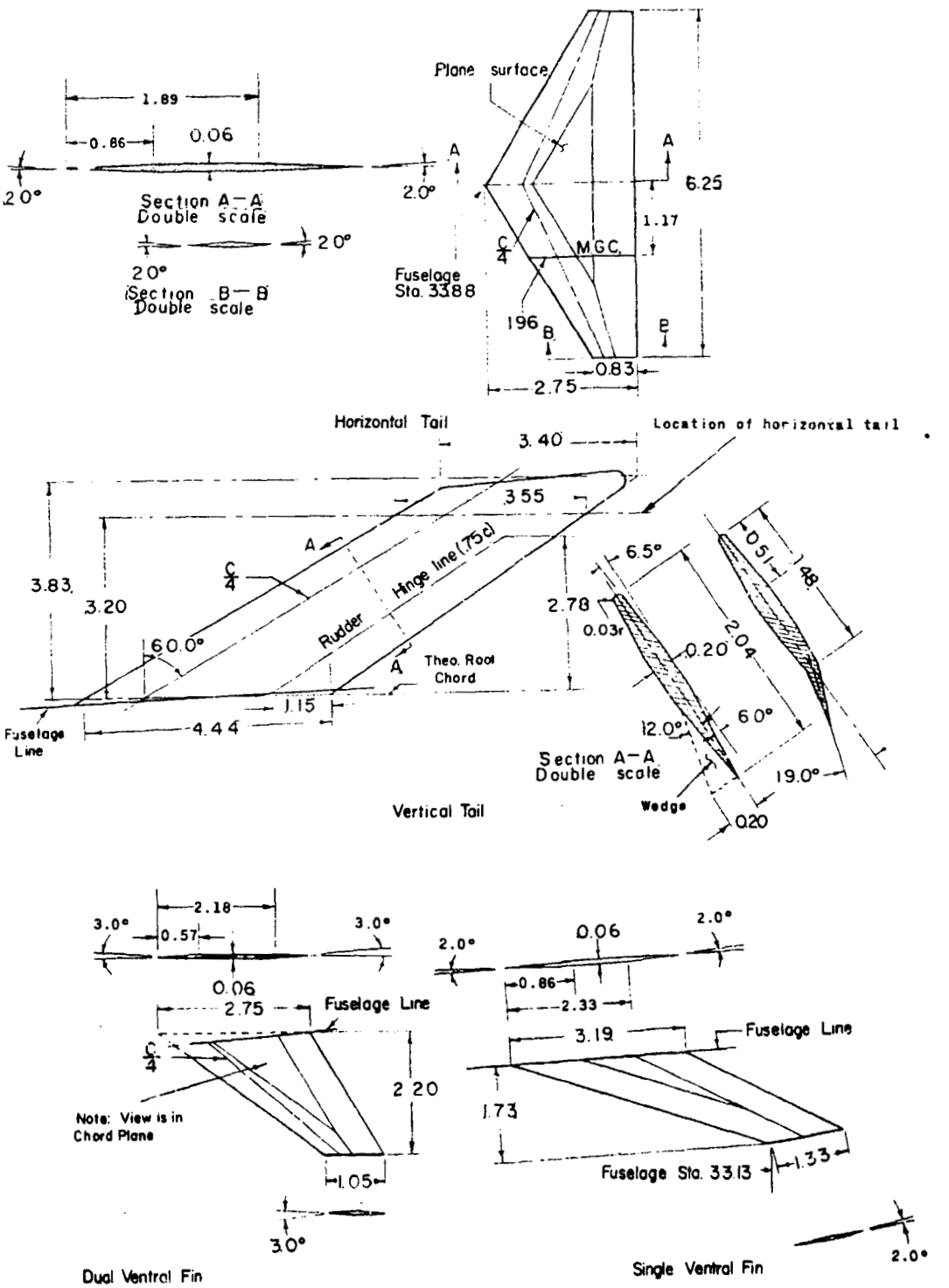

Figure 3.- Drawing of the basic T-tail components including single and dual ventral fins. All dimensions are in inches.

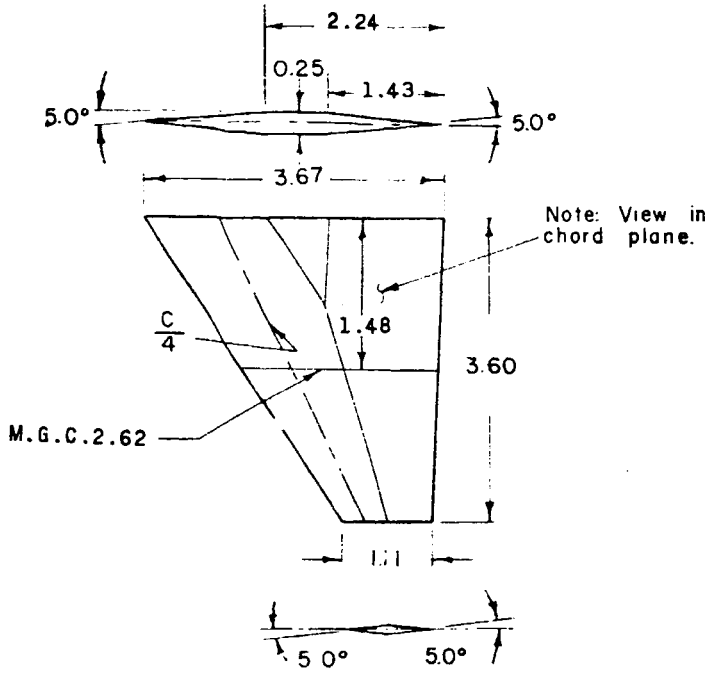

Horizontal Tail

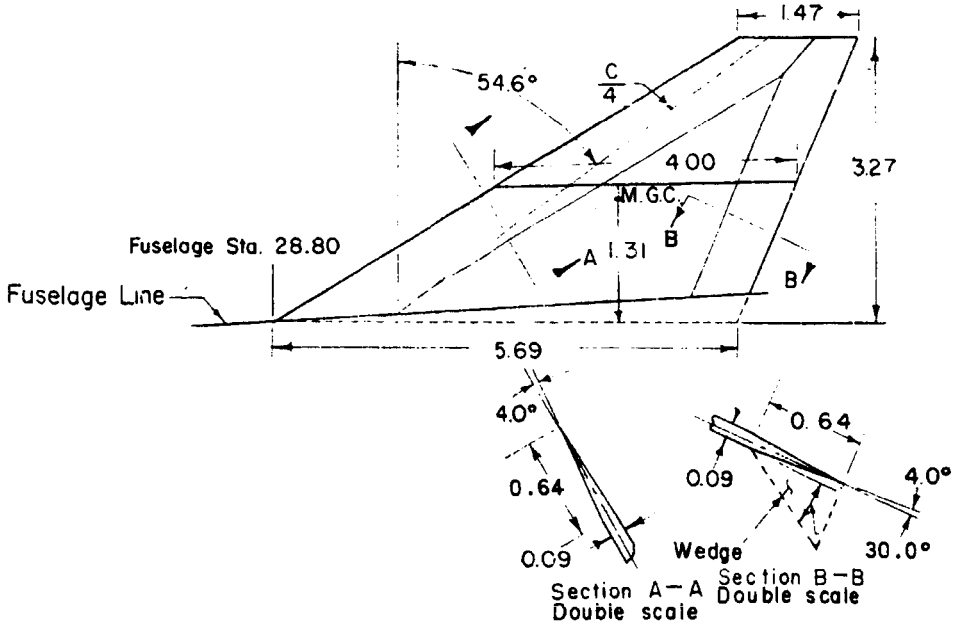

Vertical Tail

Figure 4.- Drawing of the low-tail components. All dimensions are in inches.

L-96895

(a) Rear-quarter view of model with T-tail and dual ventral fins.

Figure 5.- Photographs of a supersonic-bomber model.

L-96896

(b) Rear-quarter view of model with T-tail and single ventral fins.

Figure 5.- Continued.

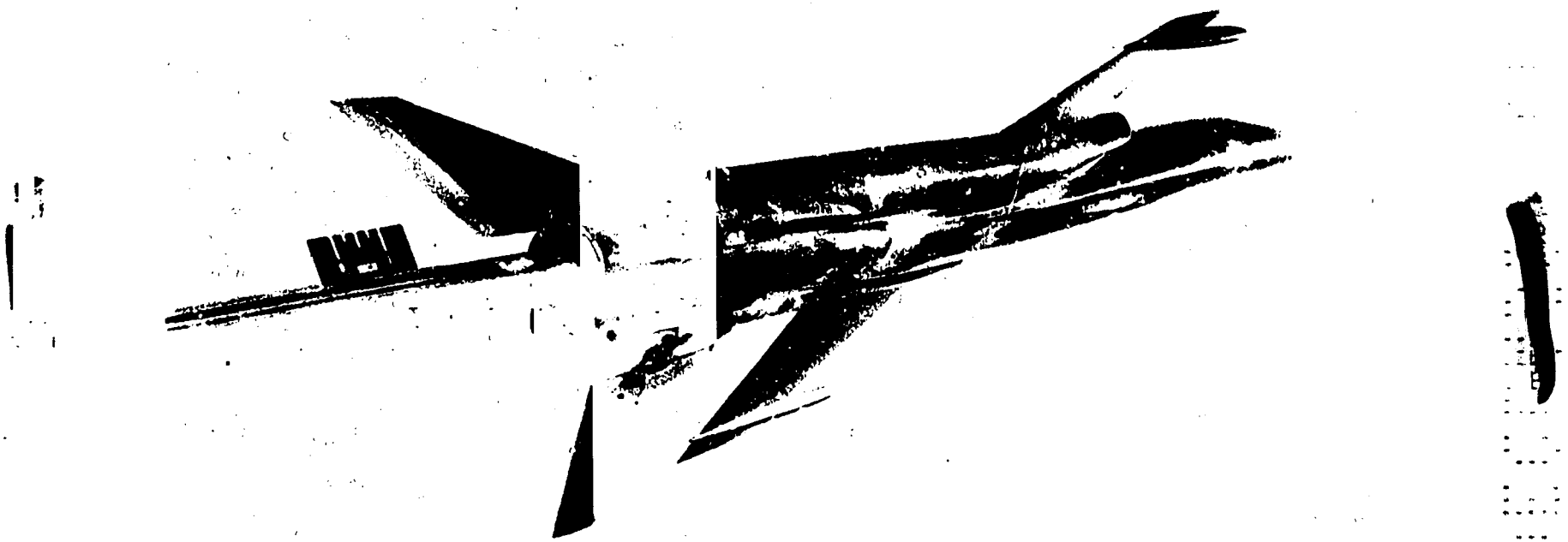

L-96897

(c) Rear-quarter view of model with low-tail configuration.

Figure 5.- Continued.

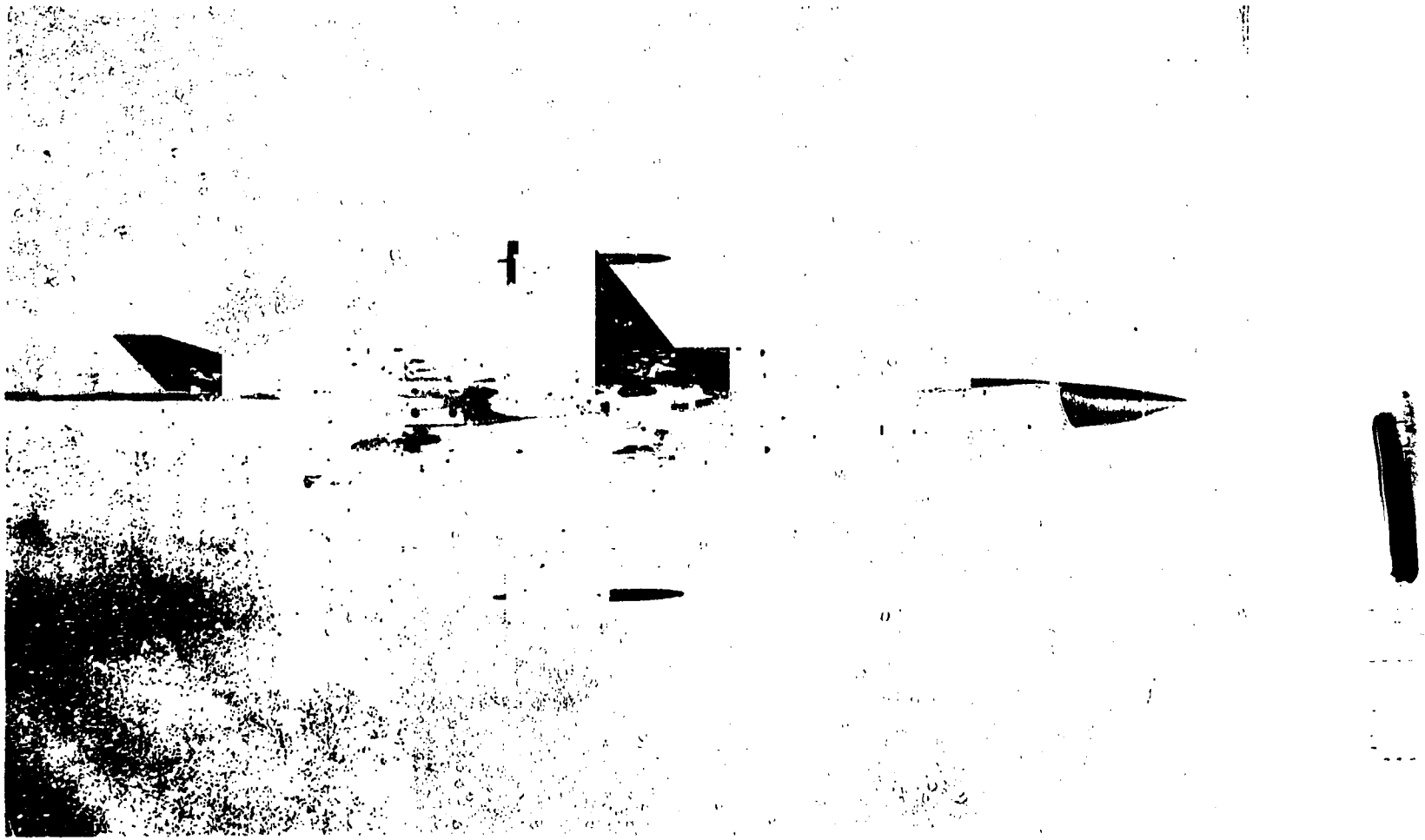

L-66899

(d) Top-quarter view of model with low-tail configuration.

Figure 5.- Concluded.

M=1.60

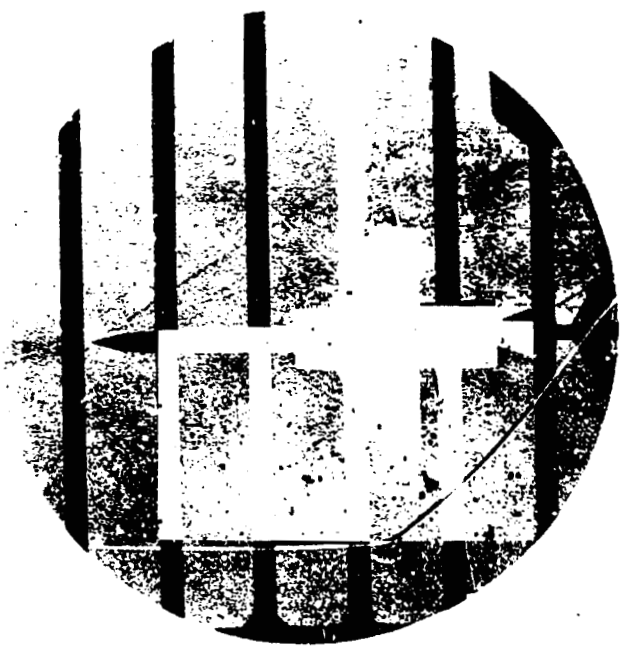

M=1.90

L-60-218

Figure 6.- Schlieren photographs of a model of a supersonic-bomber configuration in the Langley Unitary Plan wind tunnel. T-tail configuration with double ventral fins. $\phi = 0^{\circ}$; $\alpha \approx 0^{\circ}$; $\beta \approx 0^{\circ}$.

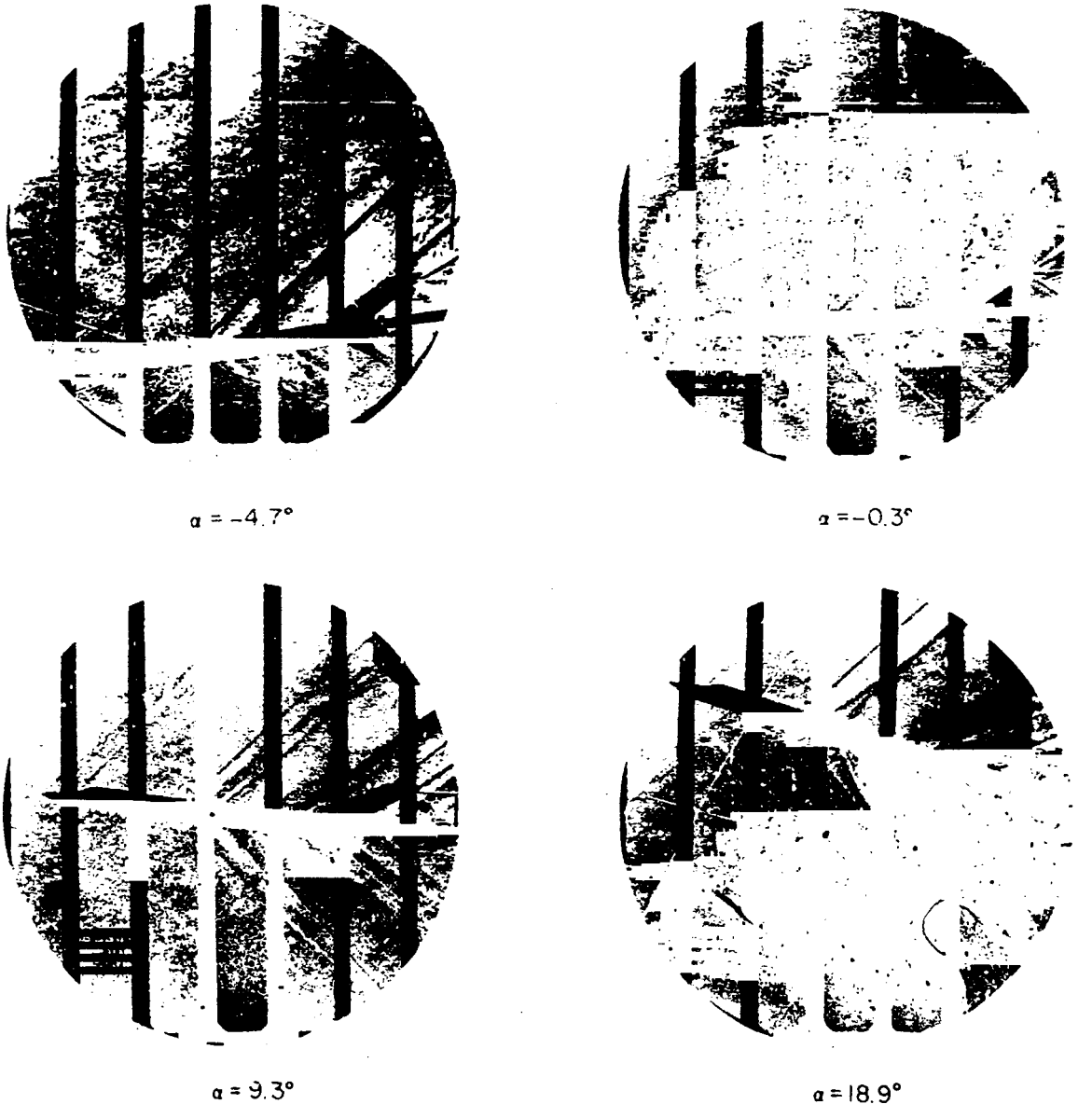

(a) M = 1.60. L-60-2139

Figure 7.- Schlieren photographs of a model of a supersonic-bomber configuration in the Langley Unitary Plan wind tunnel. T-tail configuration with double ventral fins. $\phi = 90^{\circ}$; $\beta \approx 0^{\circ}$.

$\alpha = 0.1°$

$\alpha = 9.2°$

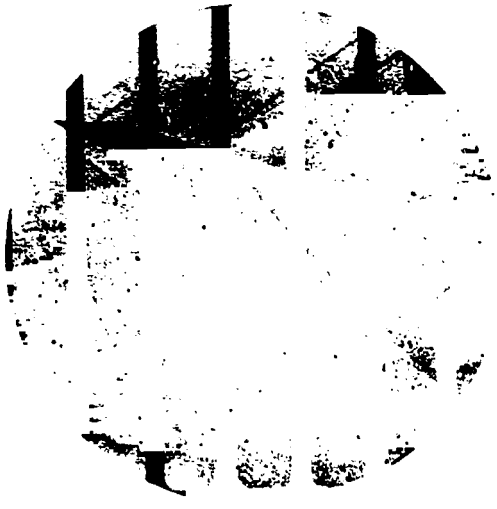

$\alpha = 18.5°$

(b) M = 1.90. L-60-220

Figure 7.- Continued.

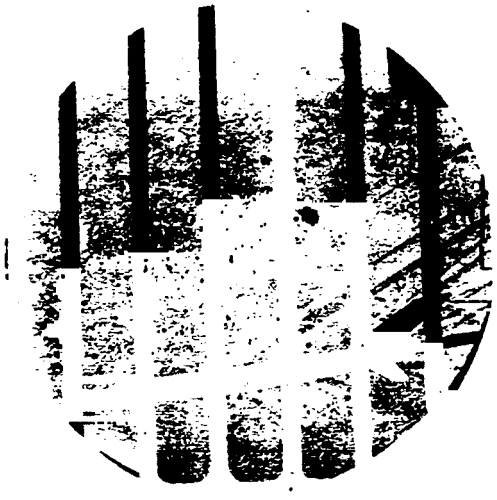

$\alpha = -4.4°$

$\alpha = 0°$

$\alpha = 9.1°$

$\alpha = 18.3°$

(c) M = 2.20. L-60-221

Figure 7.- Continued.

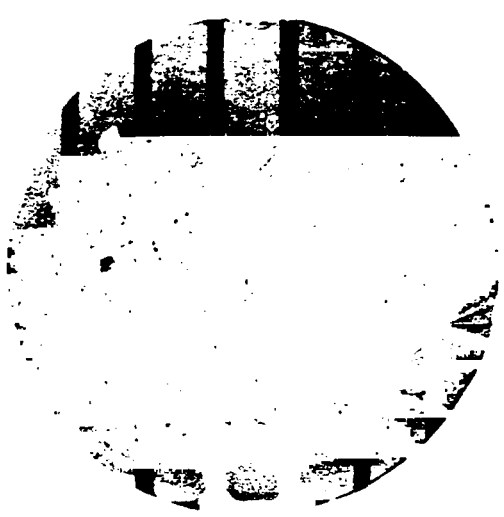

$\alpha = -4.4°$

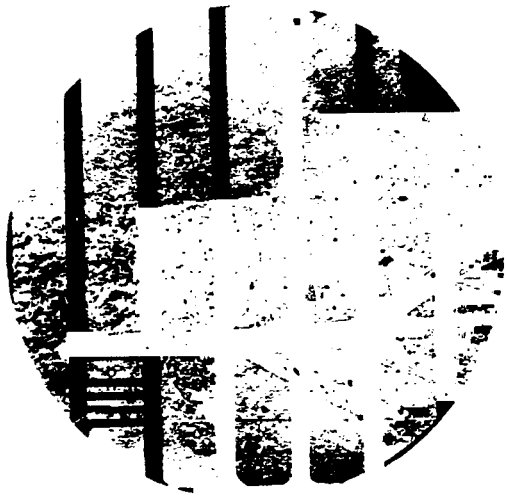

$\alpha = 0°$

$\alpha = 8.9°$

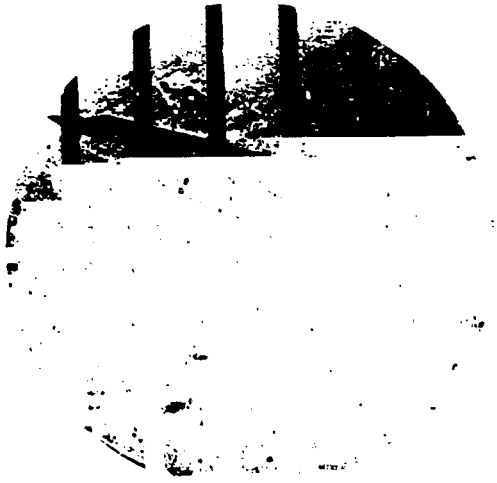

$\alpha = 17.9°$

(d) M = 2.50. L-60-222

Figure 7.- Concluded.

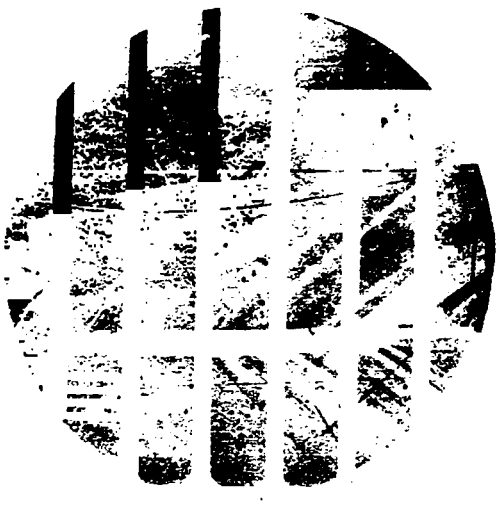

$\Gamma_t = -10.0°$

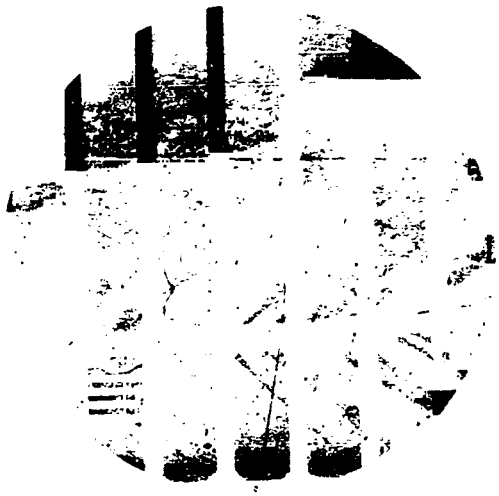

$\Gamma_t = -30.0°$

$\alpha = -0.1°$

$\alpha = 9.4°$
$\Gamma_t = -10.0°$

(a) M = 1.60. L-60-223

Figure 8.- Schlieren photographs of a model of a supersonic-bomber configuration in the Langley Unitary Plan wind tunnel. Low-tail configuration; $\phi = 90°$; $\beta \approx 0°$.

$\Gamma_f = -10.0°$ $\Gamma_f = -30.0°$

$\alpha = 0°$

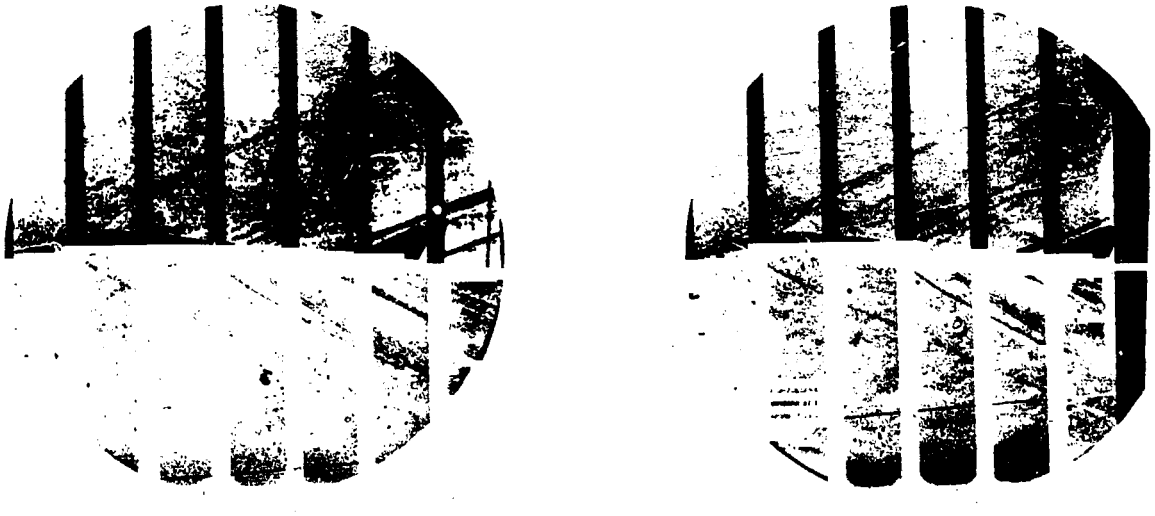

$\Gamma_f = -10.0°$ $\Gamma_f = -30.0°$

$\alpha = 10.6°$

(b) M = 2.50. L-60-224

Figure 8.- Concluded.

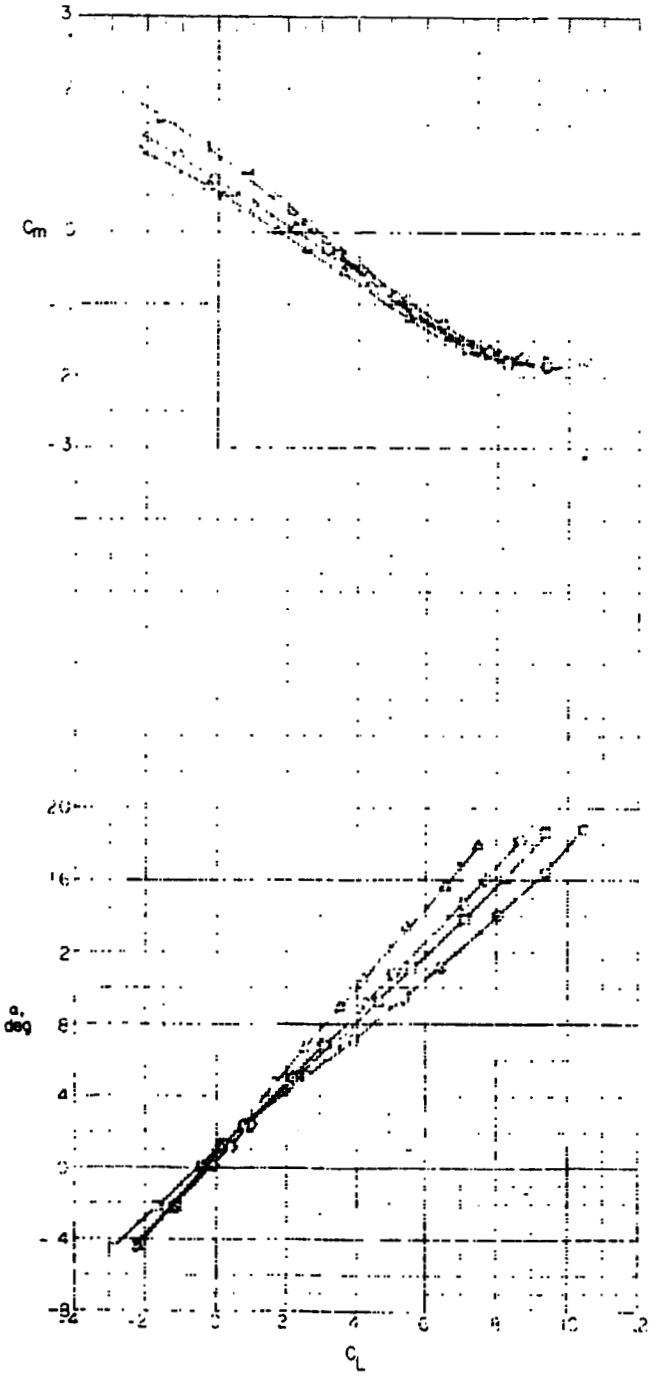

(a) Model with T-tail configuration.

Figure 9.- Longitudinal aerodynamic characteristics of a supersonic-bomber model.

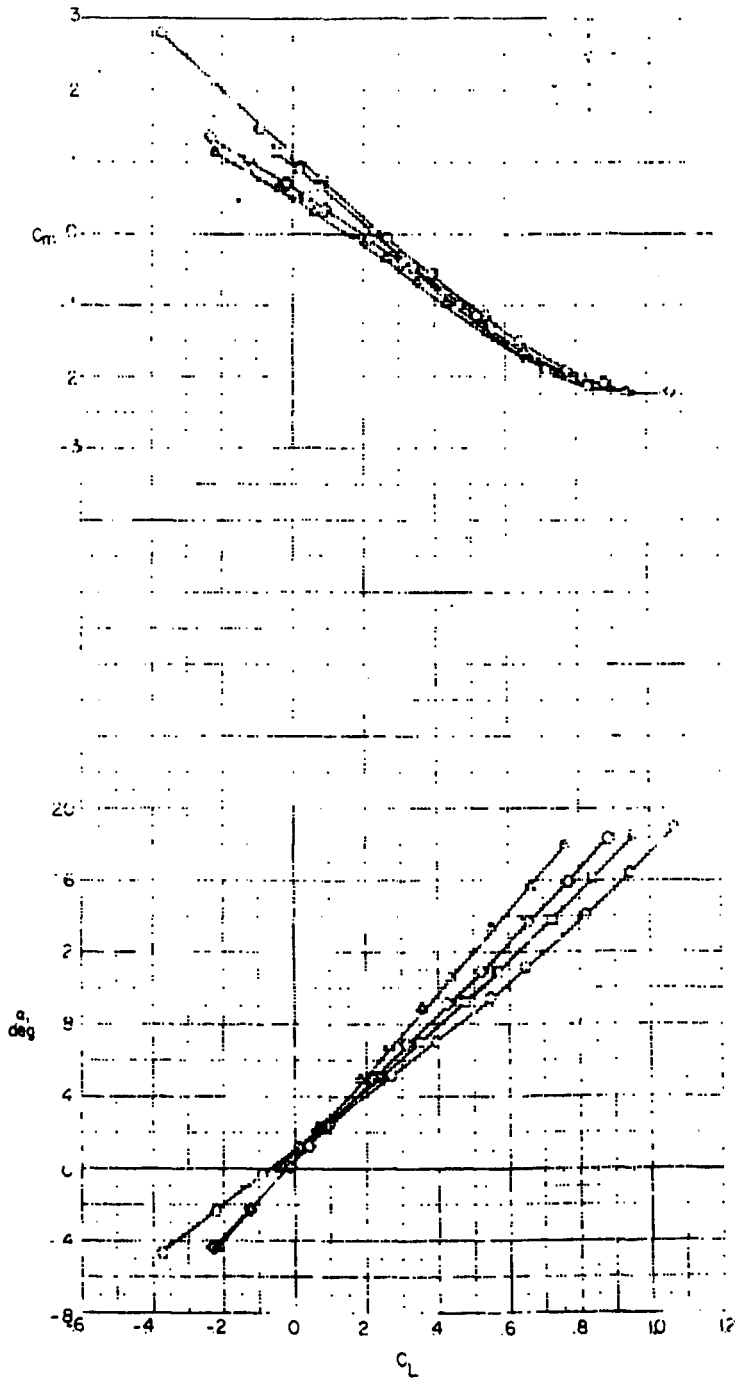

(b) Model with T-tail configuration and dual ventral fins.

Figure 9.- Continued.

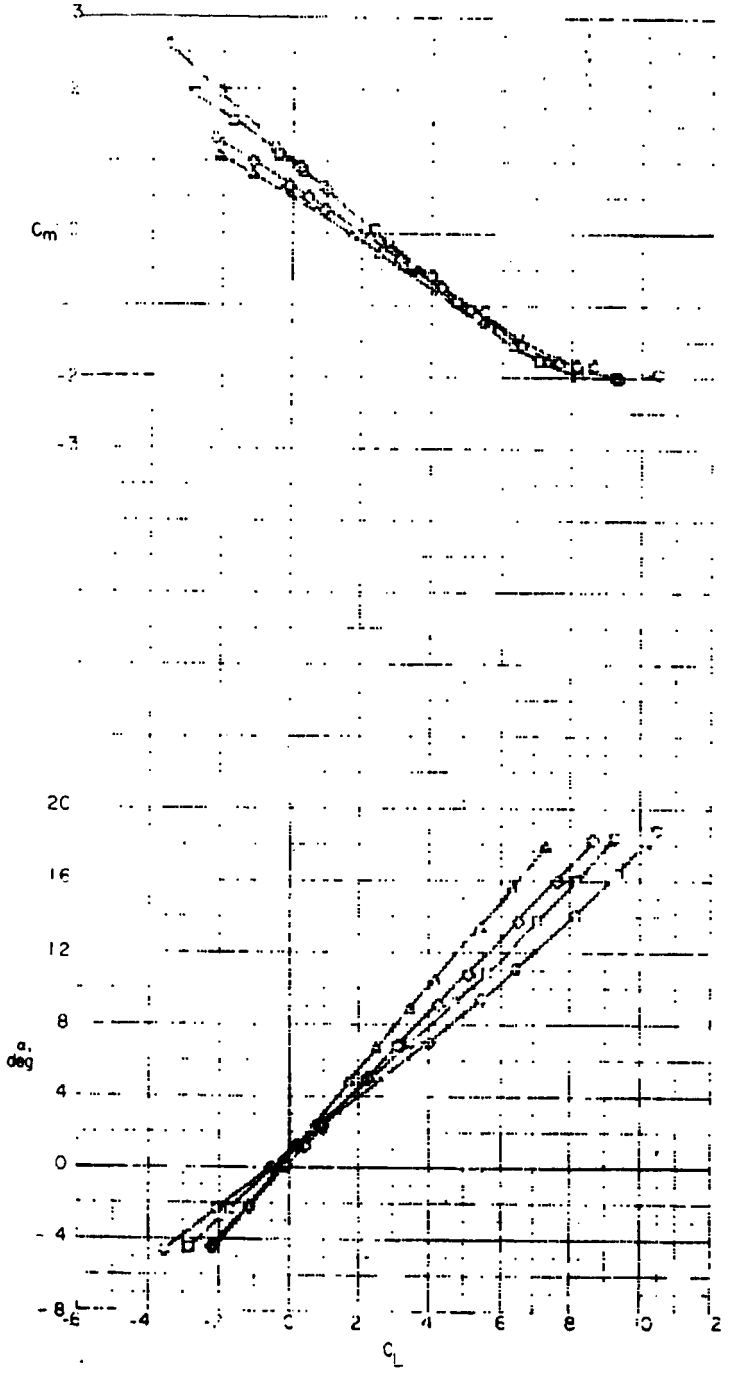

(c) Model with T-tail configuration; $\delta_r = 19^\circ$.

Figure 9.- Continued.

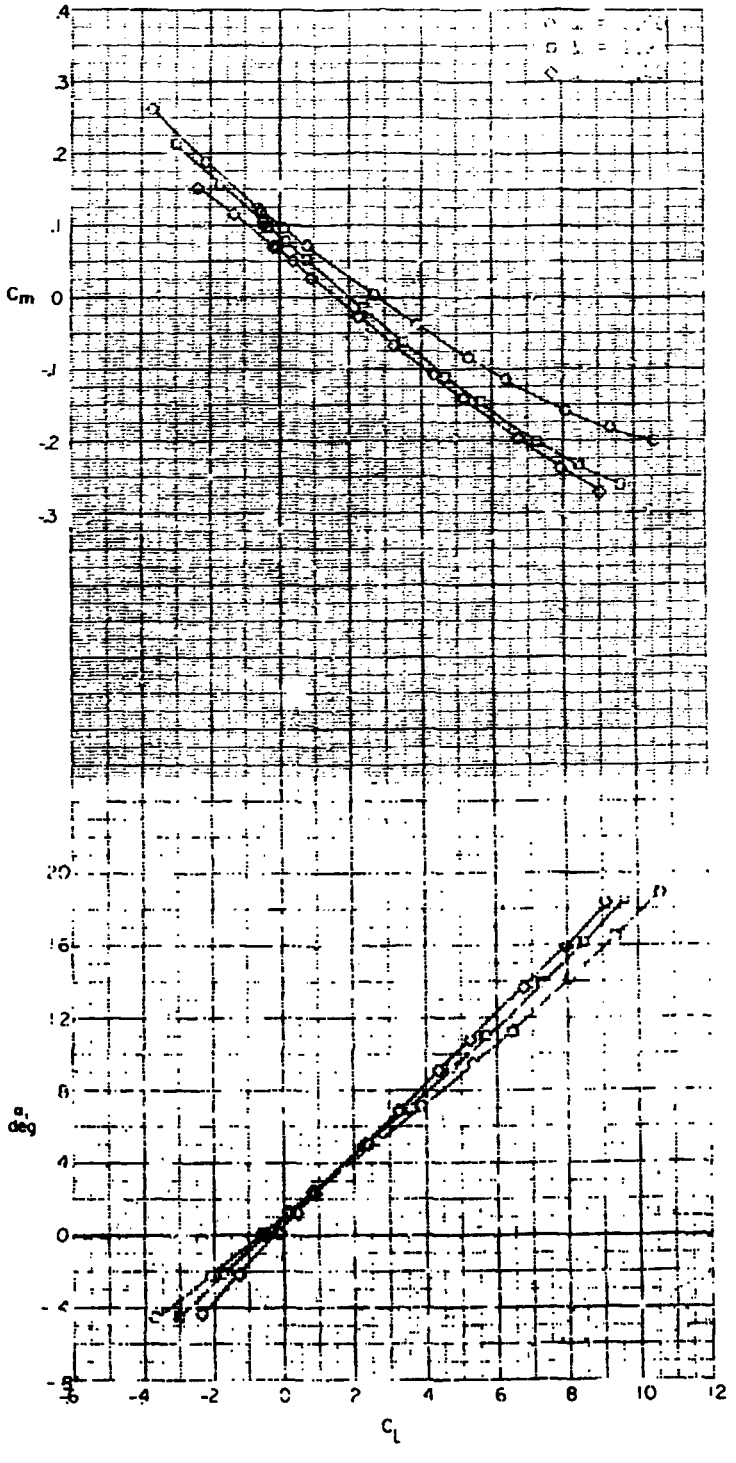

(d) Model with T-tail configuration and extended nacelle; $\delta_r = 19^\circ$.

Figure 9.- Continued.

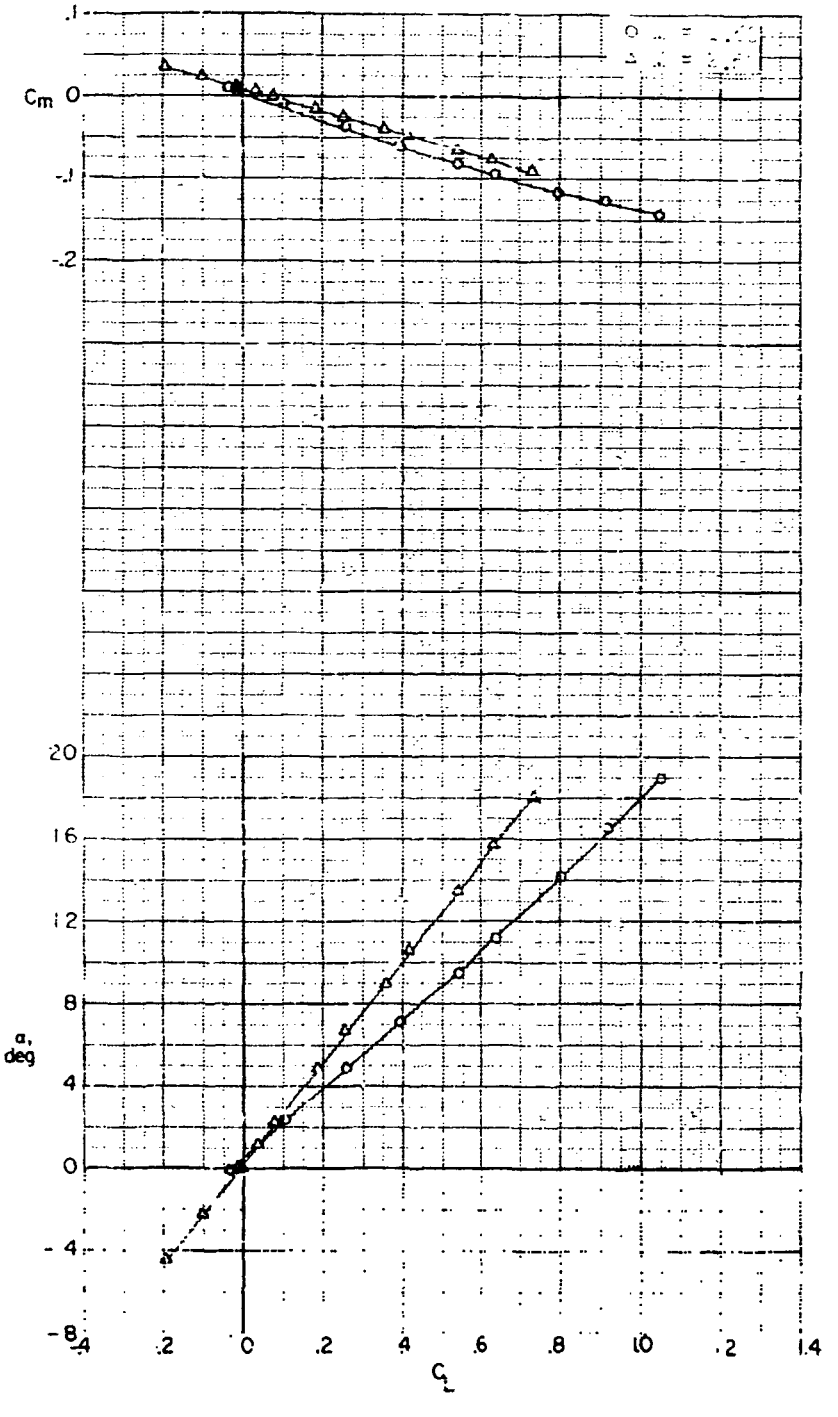

(e) Model without horizontal tail; $\delta_r = 19^\circ$.

Figure 9.- Continued.

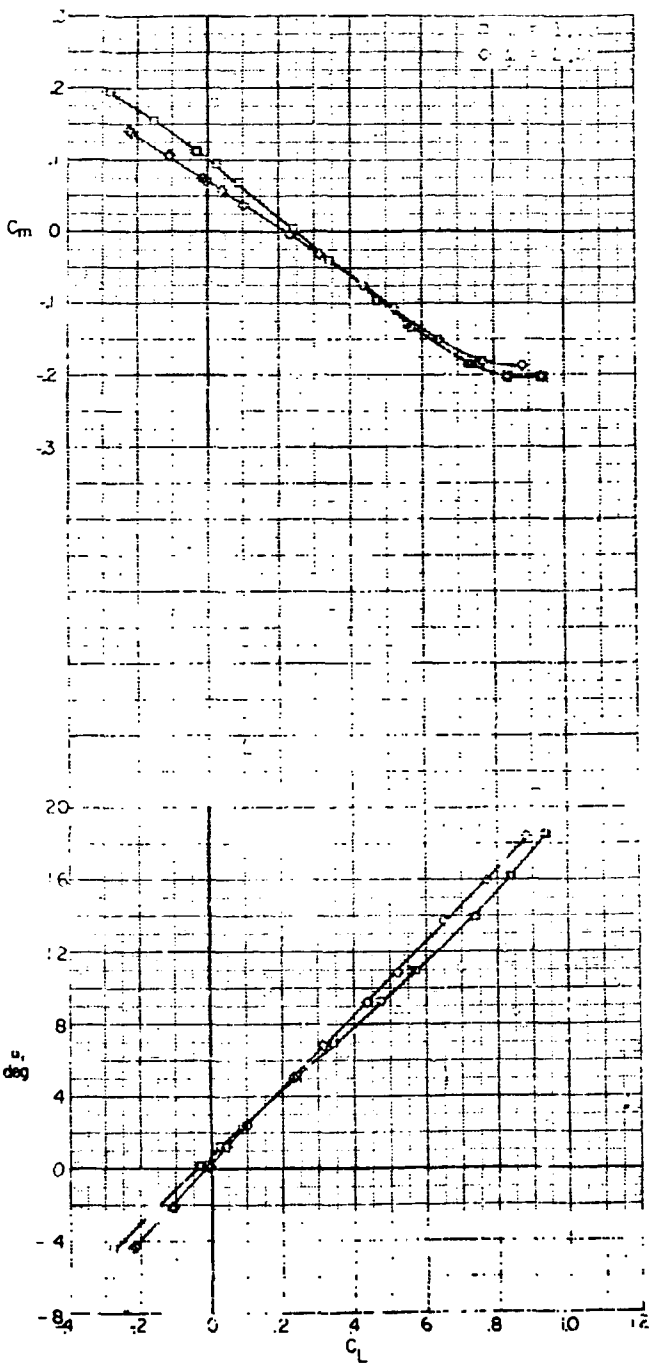

(f) Model with T-tail configuration and 12° wedge.

Figure 9.- Continued.

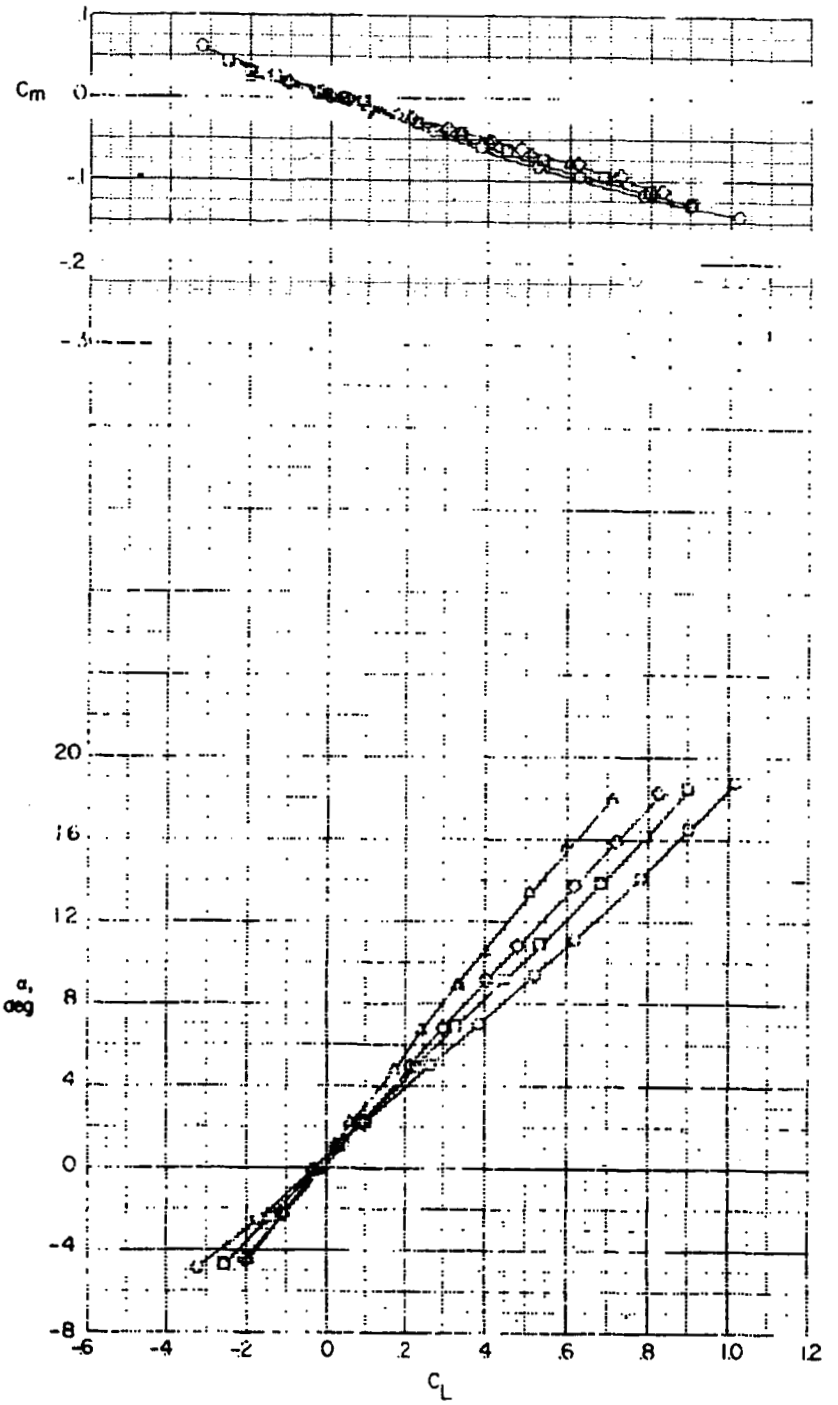

(g) Model without tail.

Figure 9.- Continued.

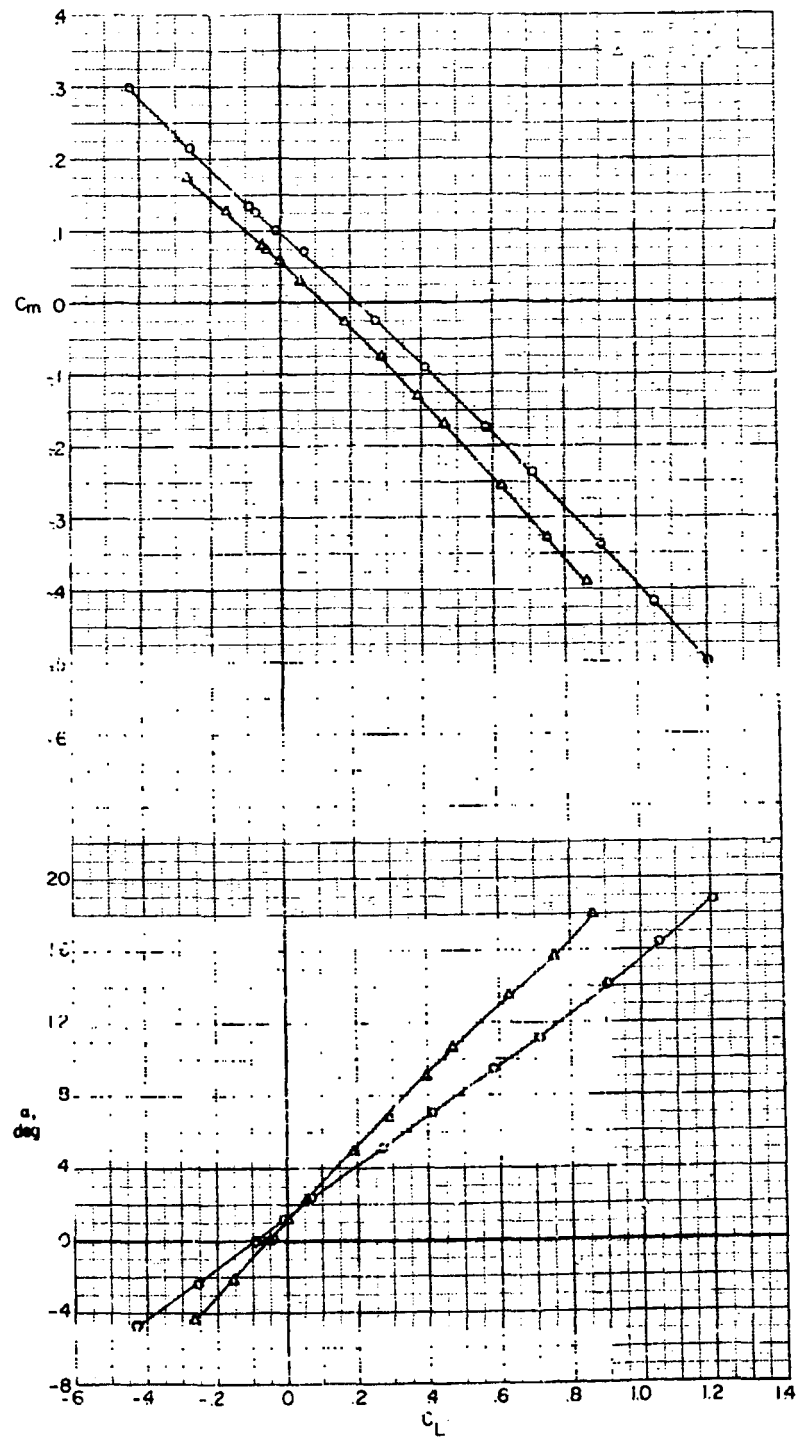

(h) Model with low-tail configuration; $\Gamma_t = -10^\circ$.

Figure 9.- Continued.

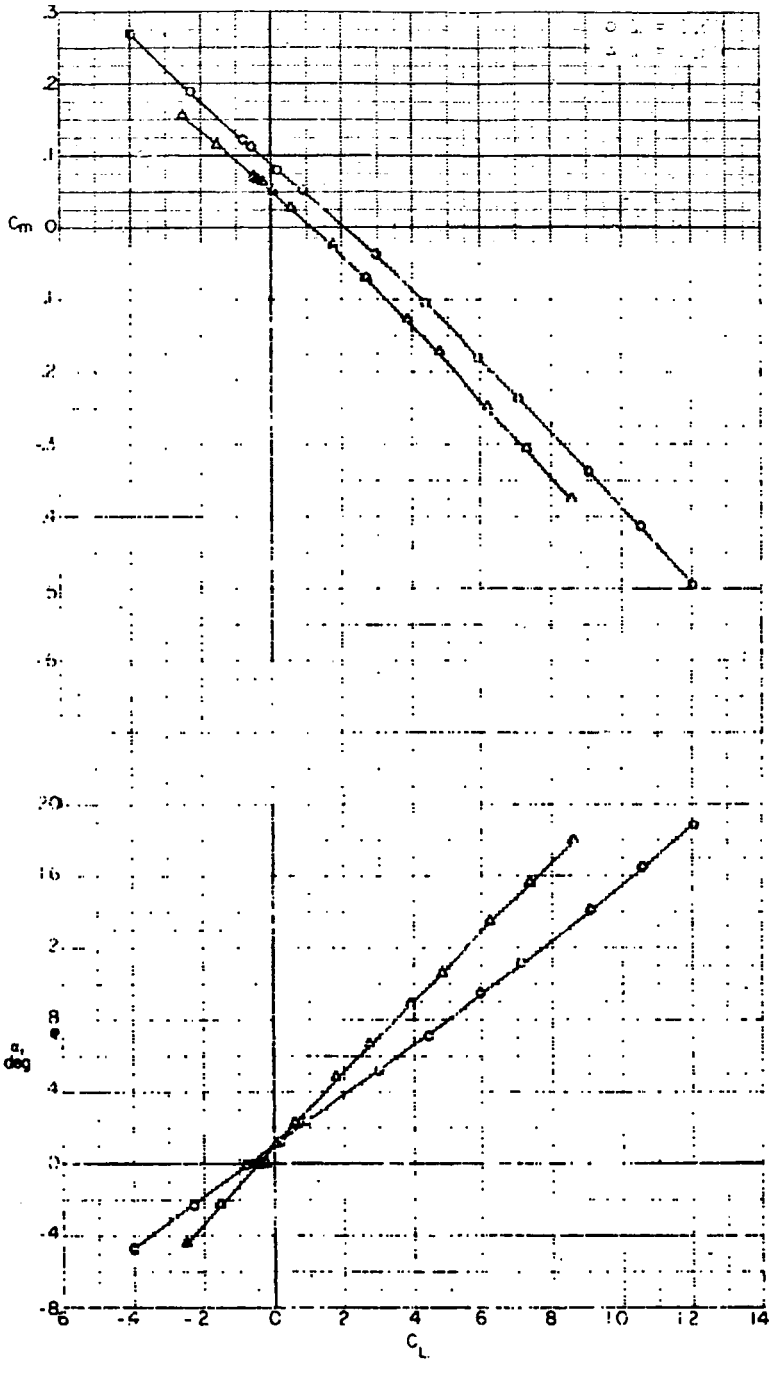

(i) Model with low-tail configuration; $\Gamma_t = -30^\circ$.

Figure 9.- Continued.

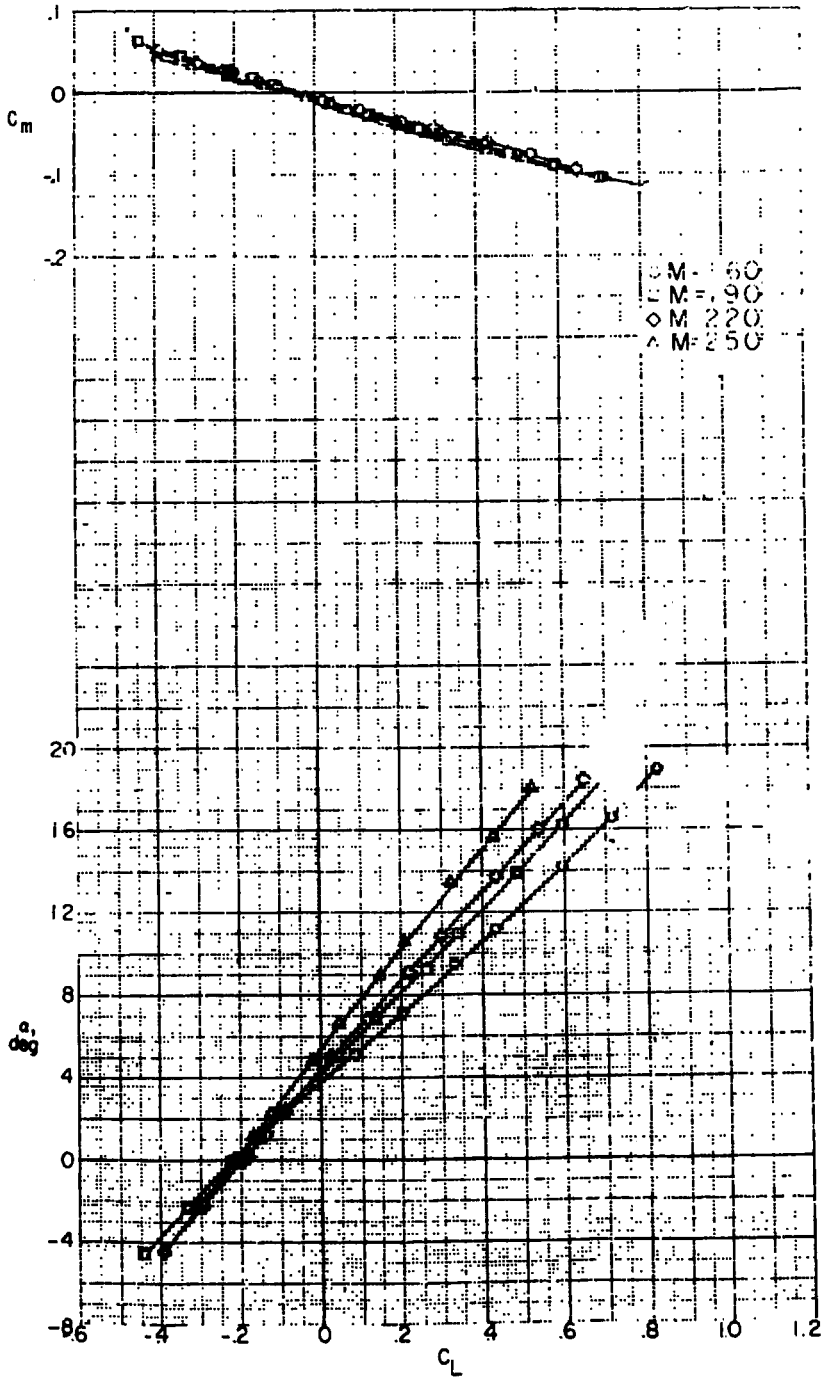

(j) Model with vertical tail of low-tail configuration and 30° wedge (without horizontal tail).

Figure 9.- Concluded.

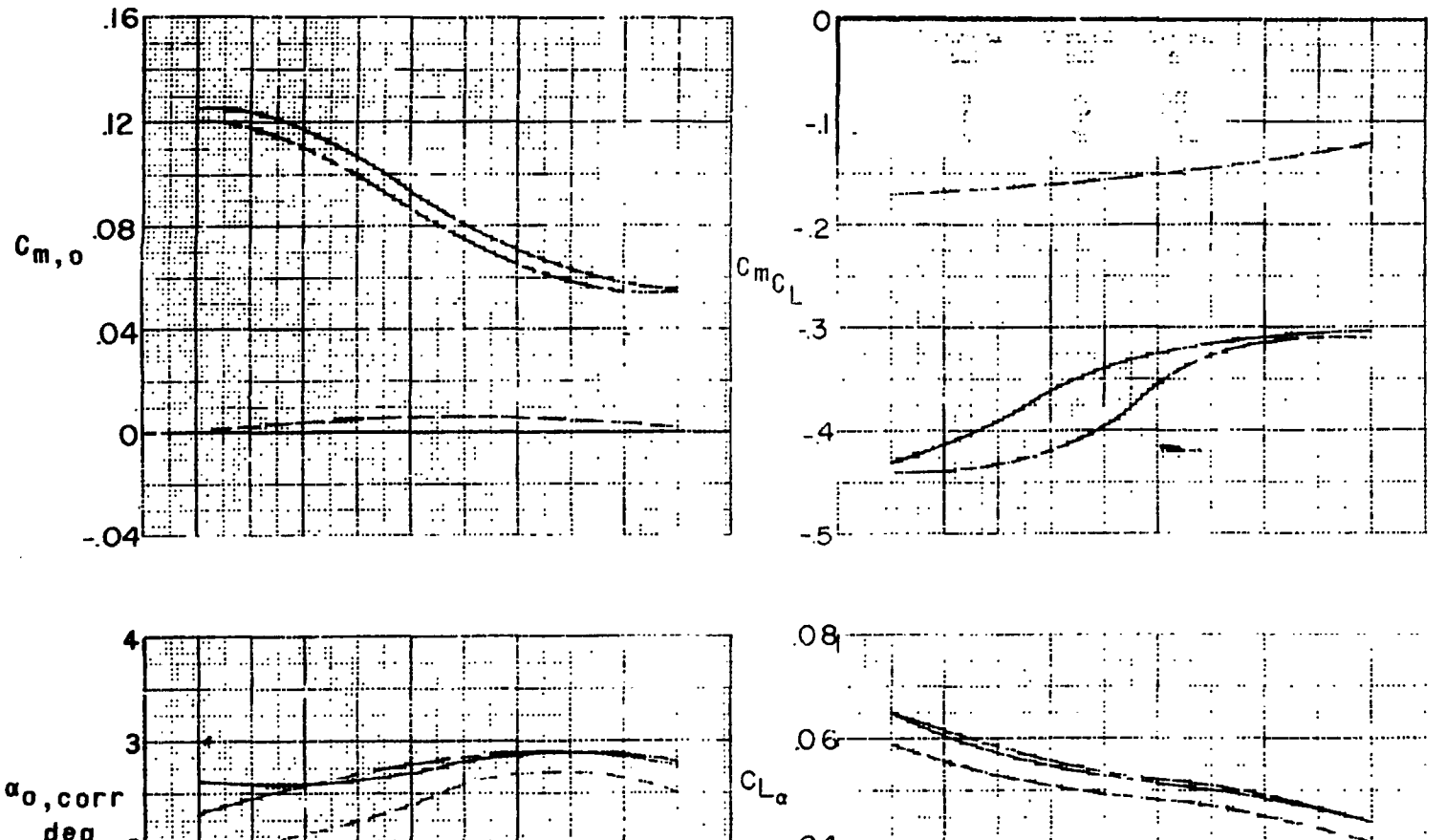

Figure 10.- Summary of longitudinal stability characteristics of a supersonic-bomber model with T-tail configuration.

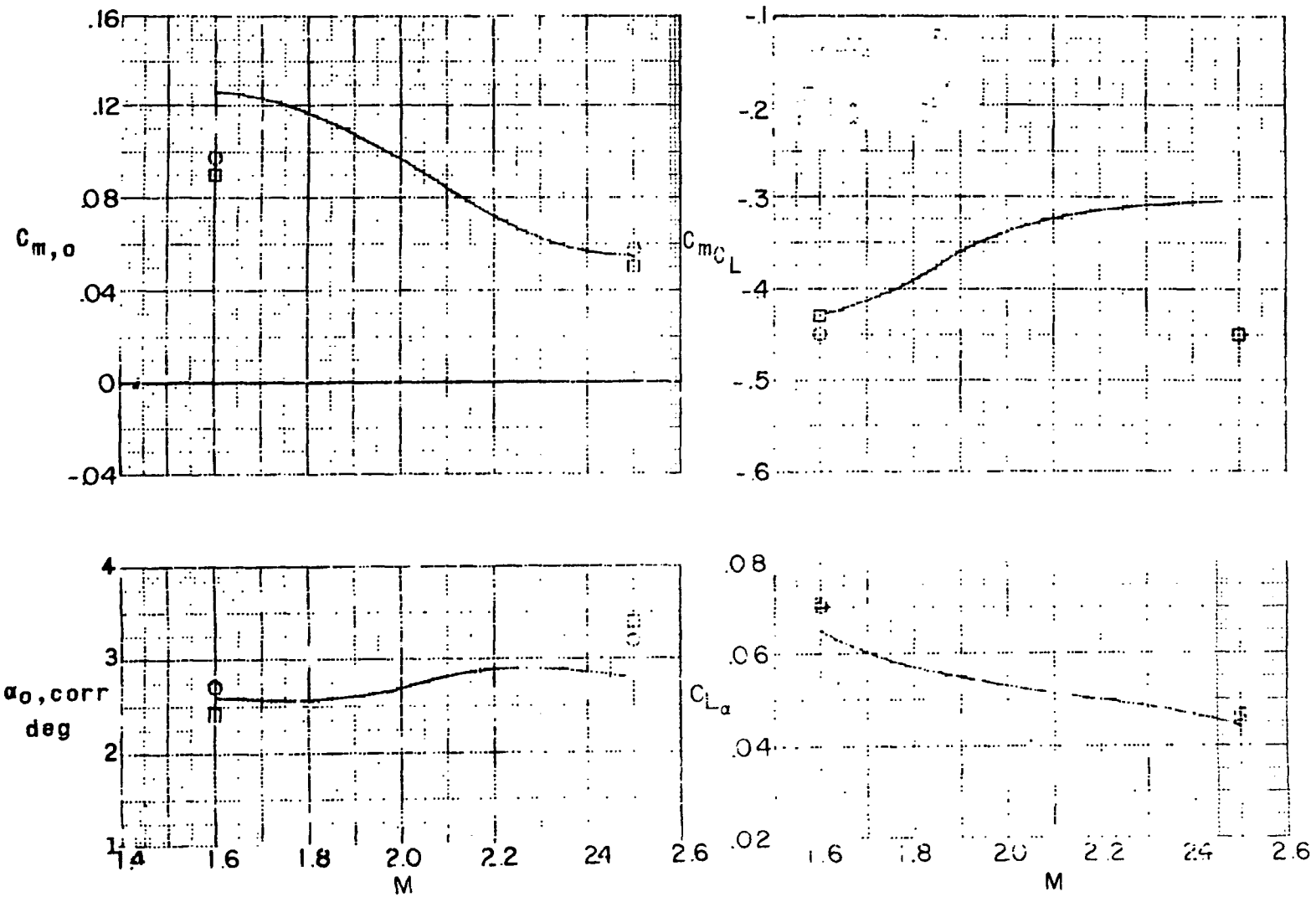

Figure 11.- Summary of the longitudinal stability characteristics of a supersonic-bomber model with T-tail and low-tail configurations.

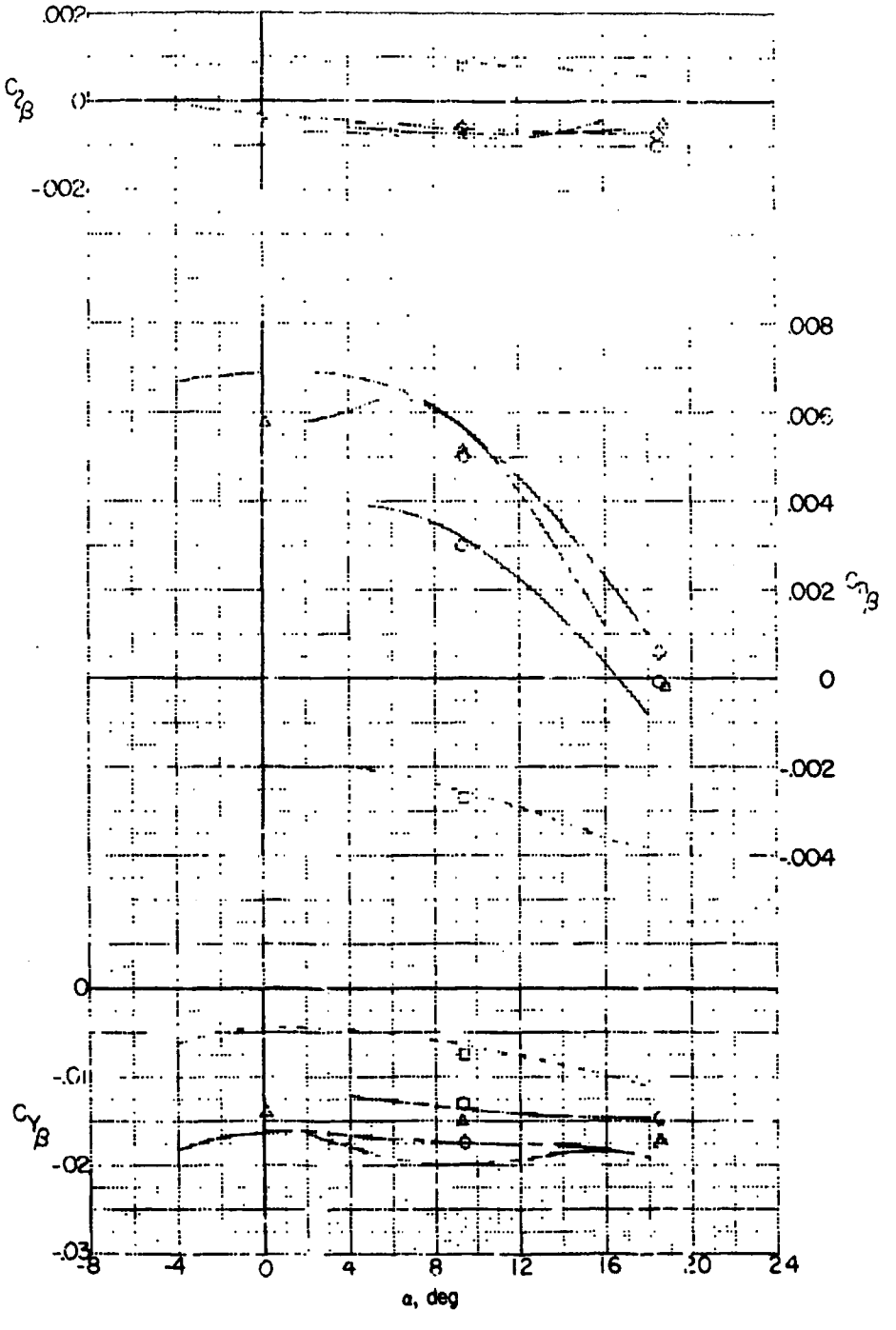

(a) M = 1.60.

Figure 12.- Lateral aerodynamic characteristics of a supersonic-bomber model. T-tail configuration. Lines denote data from parameter runs. Symbols denote points from β runs.

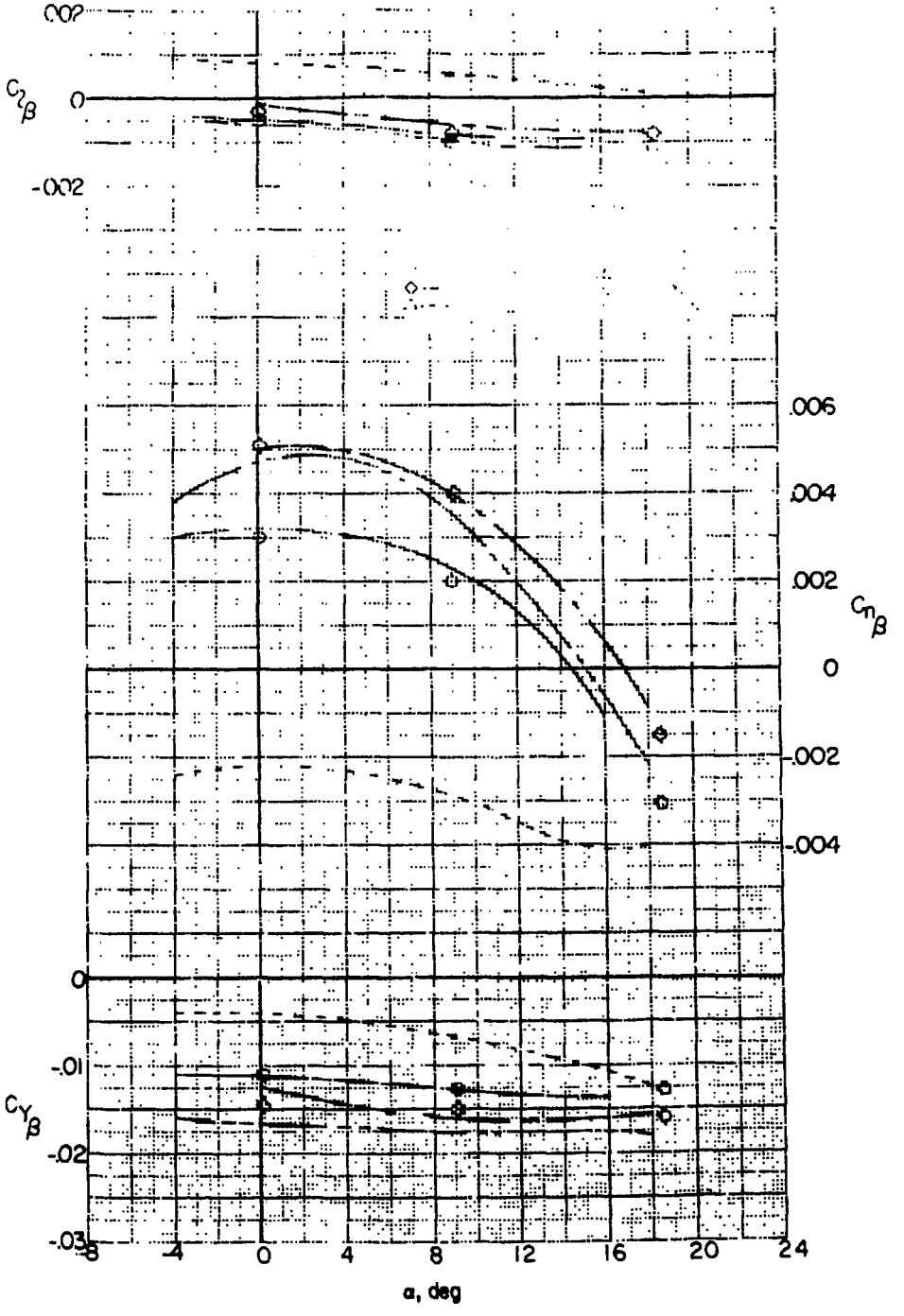

(b) M = 1.90.

Figure 12.- Continued.

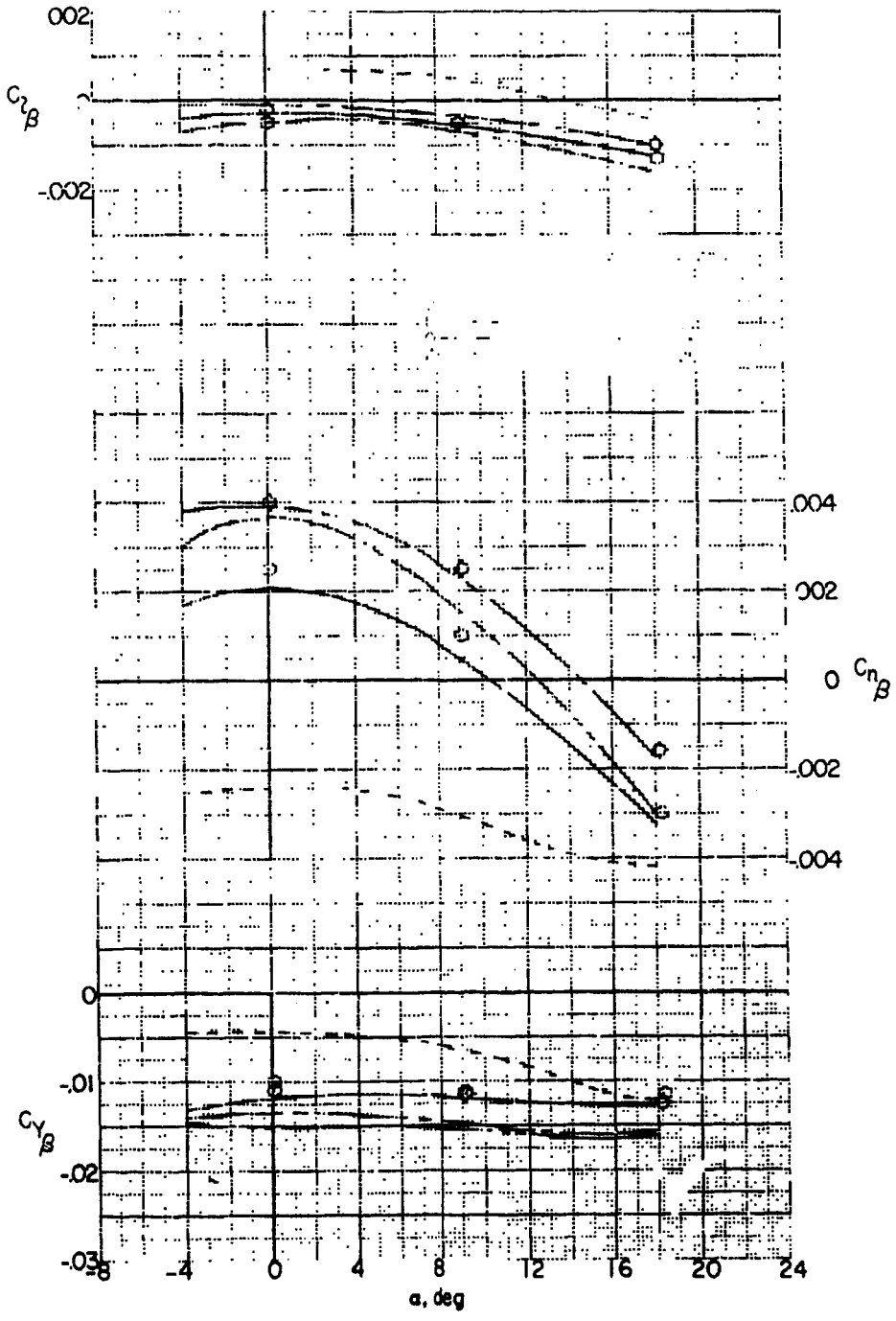

(c) M = 2.20.

Figure 12.- Continued.

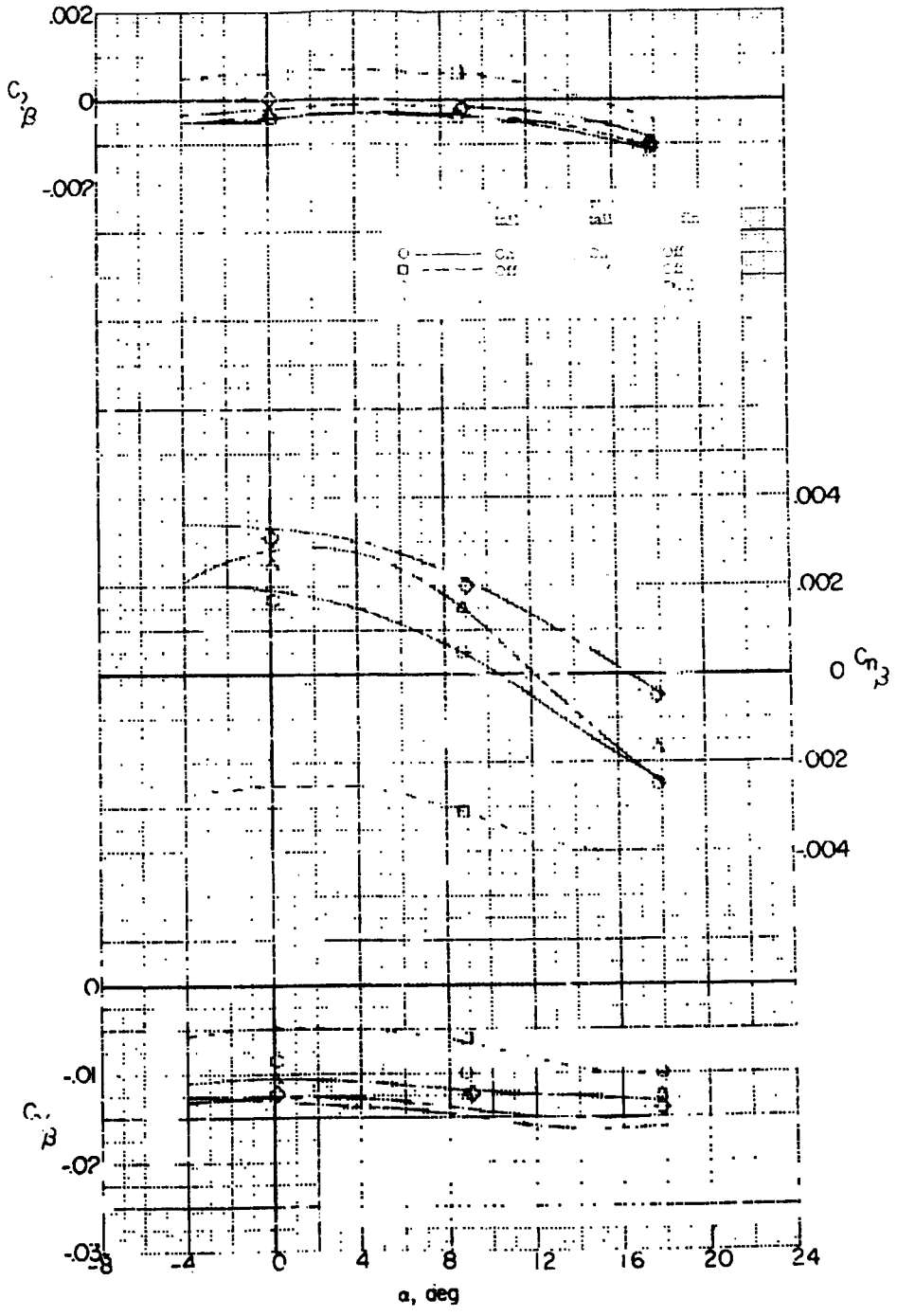

(d) M = 2.50.

Figure 12.- Concluded.

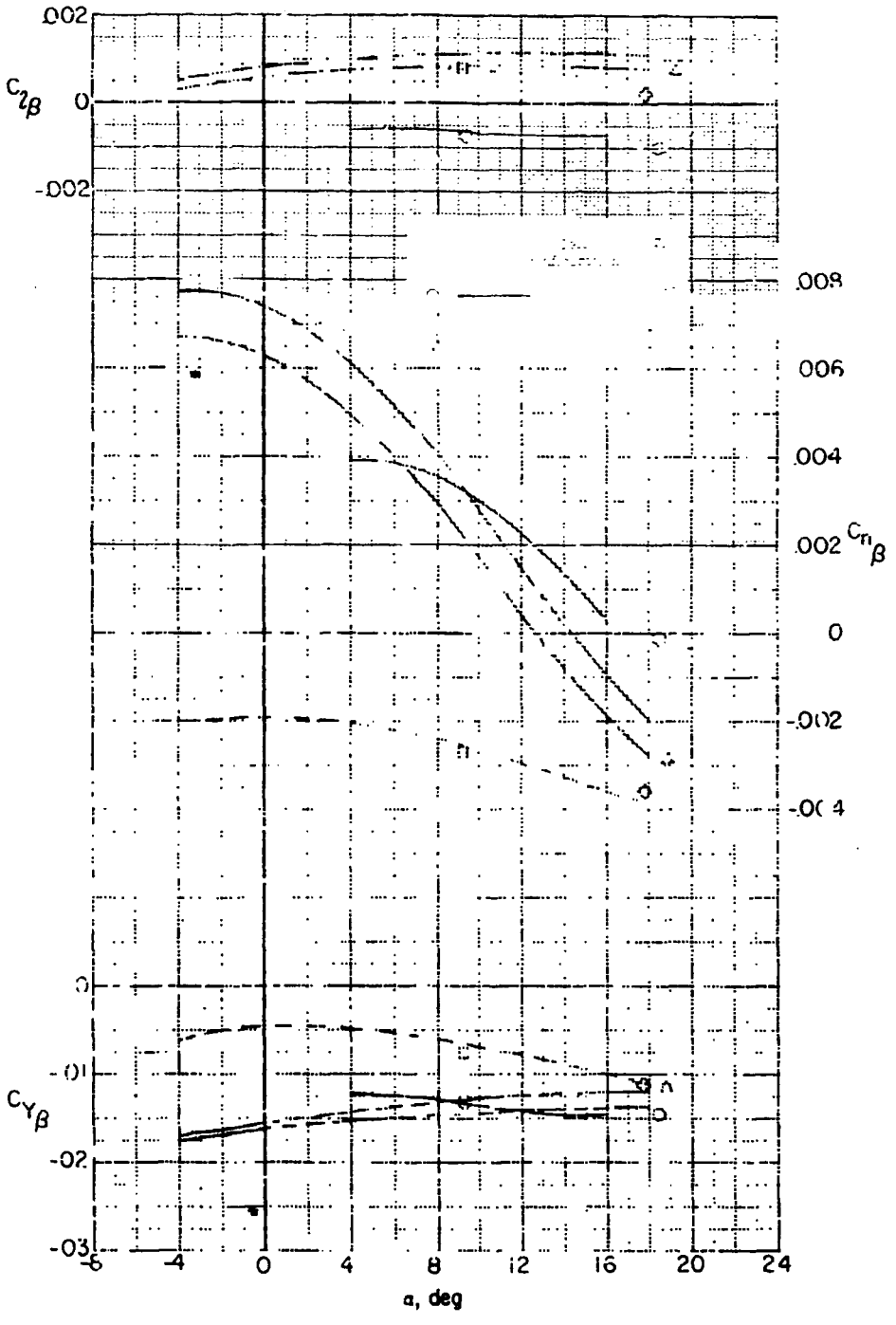

(a) M = 1.60.

Figure 13.- Lateral aerodynamic characteristics of a supersonic-bomber model. T-tail and low-tail configuration. Lines denote data from parameter runs. Symbols denote points from β runs.

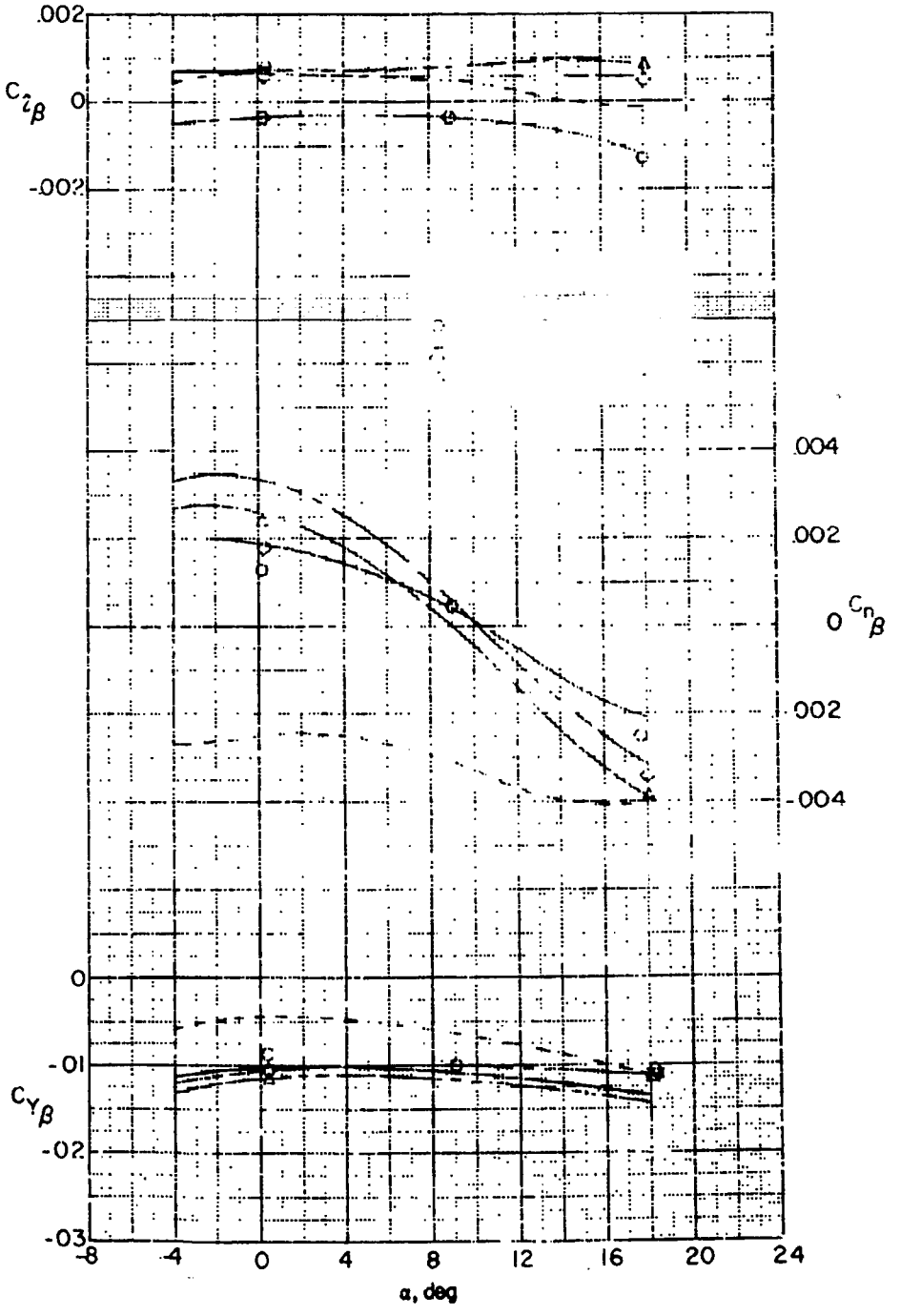

(b) M = 2.50.

Figure 13.- Concluded.

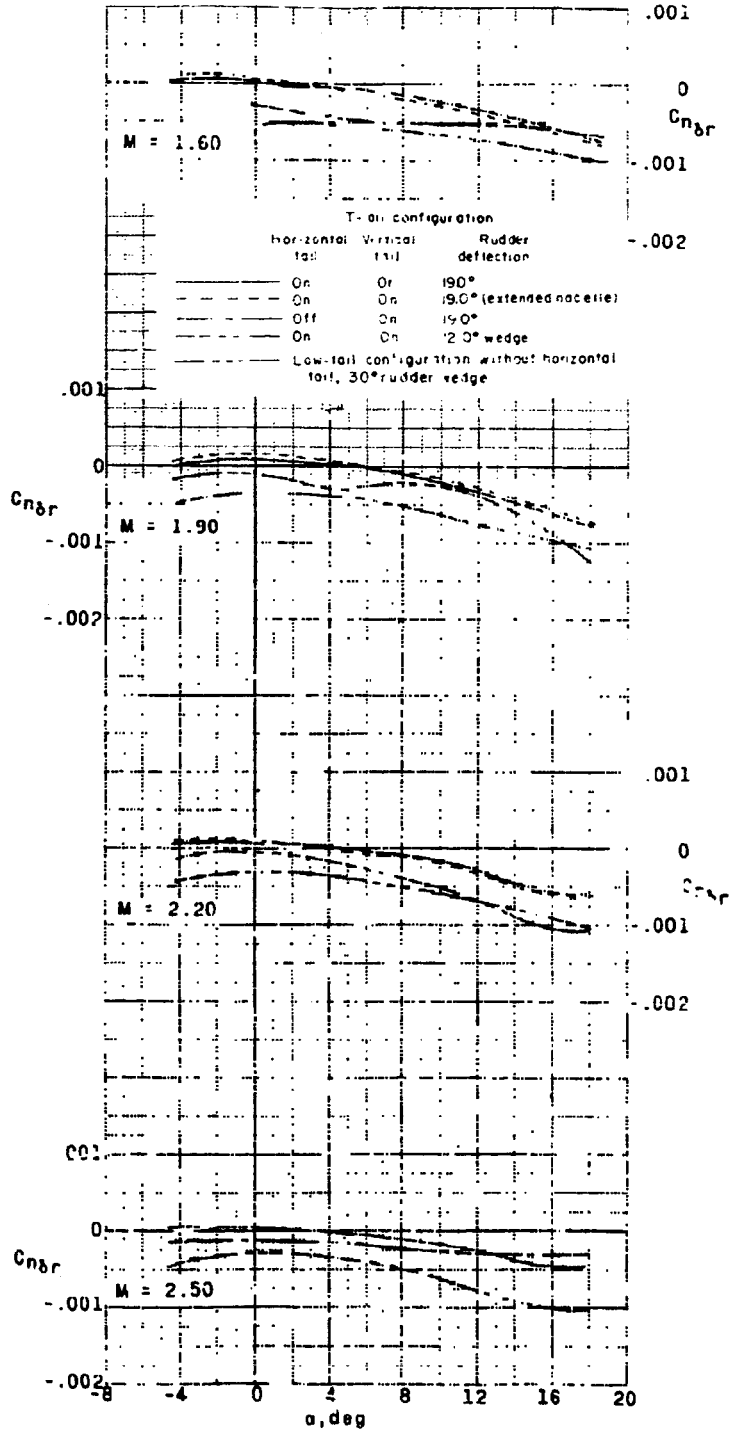

Figure 14.- Rudder effectiveness.